Low-pressure glow discharge plasma-assisted catalytic CO2 hydrogenation-The effect of metal oxide support on the performance of the Ni-based catalyst

Radoslaw Dębek, Federico Azzolina-Jury, Arnaud Travert, Françoise Mauge, Frederic Thibault-Starzyk

Low-pressure glow discharge plasma-assisted catalytic CO_2 hydrogenation – the effect of metal oxide support on the performance of the Ni-based catalyst

Radosław Dębek[a,b], Federico Azzolina-Jury[a]*, Arnaud Travert[a], Françoise Maugé[a], Frédéric Thibault-Starzyk[c]

[a] Normandie Univ, ENSICAEN, UNICAEN, CNRS, Laboratoire Catalyse et Spectrochimie, 14000 Caen, France

[b] AGH University of Science and Technology, Faculty of Energy and Fuels, Department of Fuels Technology, 30 A. Mickiewicza Avenue, 30-059, Kraków, Poland

[c] Maison Française d'Oxford, CNRS, MEAE, 2-10 Norham Rd, Oxford OX2 6SE, United Kingdom

*corresponding author: federico.azzolina-jury@ensicaen.fr

Keywords: glow discharge plasma, low-pressure, nickel catalyst, CO_2 methanation

Abstract

Low-pressure, glow discharge plasma catalytic CO_2 methanation was investigated in the presence of Ni/Al_2O_3, Ni/SiO_2 and Ni/CeO_2-ZrO_2 catalyst. The prepared samples were characterized by ICP, XRD, low-temperature N_2 sorption, H_2-TPR, dielectric constant measurement and FT-IR *in-situ* adsorption of NO, CO and CO_2. The performed characterization allowed selecting the optimal conditions of catalyst preparation as well as explaining the results of plasma-catalytic tests. The application of various supports had a significant effect on plasma properties and thus dissociation of CO_2 in the gas phase. It affected plasma stability as well, which decreased with the increasing values of the dielectric constant. Ni/Al_2O_3 sample showed the best performance in terms of CH_4 production. The positive effect on the catalytic activity in thermal CO_2 methanation was observed for Ni/Al_2O_3 and Ni/SiO_2 samples. Adsorption of probe molecules (NO, CO and CO_2) performed for fresh reduced and spent catalysts allowed to get insights into plasma-catalytic reaction mechanism and to explain the effect of plasma promotion on the performance of the catalysts in thermal CO_2 methanation.

1. Introduction

New techniques for the chemical use of CO_2 are needed for reducing human influence on the earth's atmosphere and the greenhouse effect. The recent report from the Intergovernmental Panel on Climate Change emphasizes the urgent need to decrease as much as possible our CO_2 emissions to avoid increasing the atmosphere's temperature [1]. The conversion of CO_2 into methane i.e. CO_2 methanation, attracted a lot of attention in the last years: it consumes CO_2 and would allow storing energy in a chemical form [2–4]. The process is run at atmospheric pressure by heating above 350°C in the presence of heterogenous catalyst. The search for efficient catalysts has been very intense, particularly on those using nickel as the metal, for economic reasons [2,5–7]. Catalysts based on noble metals (Rh, Ru, Pd) are also efficient, and significant activities were also observed on Co- or Fe-based catalysts. The replacement of conventional heating by cold (or rather non-equilibrium) plasmas for the catalytic hydrogenation of CO_2 was also proposed in the 90s' [8,9]. This process initially aimed at producing methanol because of the low economic interest in the production of methane from hydrogen at the time. This has changed with new environmental concerns and the production of methane could contribute to the solution.

The activation of catalytic processes by cold plasma has many possible advantages [10–14]. A non-equilibrium plasma is an ionised gas containing various activated species and high energy electrons. It is an extremely reactive medium with a moderate average temperature (depending on the type and geometry of the plasma). Such conditions allow converting CO_2 at much lower temperature than with conventional heating. Moreover, the surface of the catalyst can also be modified by the creation of new reaction sites under plasma. The solid can also reciprocally influence the plasma's properties by modifying local electric fields, by inducing micro-discharges, which in its turn can also create new excited species. A synergetic effect between the plasma and the catalyst can thus allow an efficient conversion of CO_2 at low temperature. The hybrid plasma-catalytic approach has been successfully applied to several other CO_2 consuming processes such as methane reforming [15–17] or CO_2 dissociation [18–21].

Table 1 Summary of recent research (years 2016-2018) on plasma-catalytic CO_2 hydrogenation to methane.

Catalyst	Plasma				Reaction					Ref.
	Type	f (kHz)	V (kV)	P (W)	p (bar)	t (°C)	Feed gas[a]	CO_2 conv. (%)	CH_4 yield (%)	
$Cu/\gamma\text{-}Al_2O_3$	DBD	8.7	n.d.	35	1	135	1/1; 34.6	8	0.68	[22]
$Mn/\gamma\text{-}Al_2O_3$								10.1	0.76	
$Cu\text{-}Mn/\gamma\text{-}Al_2O_3$								9.2	0.63	
$15Ni/\gamma\text{-}Al_2O_3$	DBD	n.d.	30	30	1	150	4/1; 69	29	1.15	[23]
							4/1+Ar; 69.2	56	4.15	
Ni(Mg,Al)O	DBD	41	10-15	16	1	160	4/1; 200	78	77	[24]
Ni-Ce(Mg,Al)O						220		16	3	
Ni-Zr(Mg,Al)O						240		70	55	
Ni-Ce,Zr(Mg,Al)O						260		68	56	
$15Ni/Ce_{0.1}Zr_{0.9}O_2$	DBD	40-41	10-15	1-3	1	320	4/1 ; 200	72	71.8	[25]
$15Ni/Ce_{0.6}Zr_{0.4}O_2$								81	80.4	
$15Ni/Ce_{0.9}Zr_{0.1}O_2$								83	82.8	
15Ni/CZ-cal[b]	DBD	40-42.8	13-18	14	1	170	4/1 ; 200	73	73	[26]
15Ni/CZ-red[b]				16		170		80	75	
$6Ru/\gamma\text{-}Al_2O_3$	DBD	3	9	n.d.	1	25	3/1/6[c] ; 50	12.8	9.4	[27]
14Ni/USY(40)	GD	0.05	2	n.d.	$3.2\cdot10^{-3}$	125	4/1 ; 20	64	2.5	[28,29]
14Ni/USY(30)								63	1.2	
2.5Ni/ZSM-11								64	1.4	
5Ni/ZSM-11								64	0.9	
Cs-USY(38)	DBD	25-70	0-15	35	1	170	36/9/ 10[c]; 250	12	1.5	[30]
$10Ni/\gamma\text{-}Al_2O_3$								61	57	
15Ni/Cs-USY(3)								22	17.6	
15Ni/Cs-USY(38)								75	72	
Ce-Ni/Cs-USY(38)								79	77.4	
$5Co/CeZrO_4$	DBD	1	n.d.	n.d.	1	150	4/1; 25	70	69.3	[31]
						200		78	77	
$1Pt/\gamma\text{-}Al_2O_3$	DBD	9	30	10	1	25	3:1; 40	18	0.3	[32]
$15Cu/\gamma\text{-}Al_2O_3$								21	0.5	

DBD – Dielectric Barrier Discharge; GD – Glow Discharge

[a] Feed gas: H_2/CO_2 molar ratio; total flow (Nml/min)

[b] CZ – Ceria-Zirconia; catalysts differed in activation: cal – calcination only; red – temperature reduction; Predx – plasma reduction for x=20, 40 or 60 min

[c] $H_2/CO_2/N_2$

Most of the work on plasma assisted catalytic methanation of CO_2 was published in the last 4 to 5 years. A summary of the various processes reported is presented in Table I. Most of them deal with the use of nickel catalysts in a dielectric-barrier discharge plasma (DBD) under atmospheric pressure. Only Zeng [22] used other solids such as Cu or Mn on alumina, obtaining only a limited production of CH_4. This might suggest that catalysts need to be efficient under conventional heating (and thus not Cu or Mn based) to be active under plasma. Under conventional heating, supporting the Ni on

ceria or on ceria-zirconia, rather than on any other oxide, often leads to a significantly better activity [33–37]. The reason for that is probably the specific interaction between Ni and ceria which allows the formation of very small and well dispersed Ni crystallites with acid-basic properties. Basic sites with intermediate basic strength are often mentioned for an important production of CH_4 [38–41]. Ce-Zr was thus also used as a support in plasma-assisted catalysis, but no formal comparison was ever done [13,25,26,31]. Plasma assisted catalysis involves complex processes, and a simple transfer of the conditions from conventional heating to plasma might in fact simply not be relevant. A thorough and direct comparison of the various supports and their influence in the plasma processes is thus necessary.

The aim of the present work was to evaluate the influence of various metal oxide supports on the catalytic performances of nickel catalysts in the methanation of CO_2 under plasma. The supports employed were alumina, silica and ceria-zirconia. Alumina and silica are common supports for catalysis, and Ni/Al_2O_3 has already been used at the pilot scale for the thermal methanation of CO_2 [42]. As already mentioned, Ce-Zr is an excellent support for this process [35]. Our comparison will tell whether the efficiency ranking of the various catalysts is the same under thermal or plasma activation. The materials were tested at room temperature in a glow-discharge reactor under low pressure. Low pressure minimizes the formation of carbon deposits, increases the life-time of excited species and stabilises the performances of the plasma in order to compare the various catalysts efficiently.

2. Experimental

2.1. Catalyst preparation

2.1.1. Supports

Alumina and silica support were commercial carriers purchased from SASOL and Solvay (Zeosil® 1165MP), respectively. Ceria-zirconia support was synthesized *via* the homogeneous urea precipitation method according to the procedure described by Pan *et al* [38]. In this procedure equimolar amounts of $Ce(NO_3)_3{\cdot}6H_2O$ and $ZrO(NO_3)_2{\cdot}5H_2O$ were dissolved in distilled water, moved to 1dm^3 round-bottom flask and aged for 3h. Subsequently, an appropriate amount of urea was dissolved in distilled water and added to the round-bottom flask. (Ce^{3+}+Zr^{4+})/urea molar ratio was equal to 1/3. The flask was immersed in an oil bath at 120°C. The prepared solution was boiled for 2h, cooled down to room temperature and filtered. The obtained material was washed with distilled water and ethanol (both ca. 0.5 dm^3) and dried at 80°C for 16h. Finally, support was calcined under

static air in a muffle oven at 500°C for 2h. The obtained ceria-zirconia support with Ce/Zr atomic ratio equal to 1 was marked as CZ.

2.1.2 Nickel-based catalysts

Nickel species were introduced onto three supports by wet impregnation method using an aqueous solution of $Ni(NO_3)_2 \cdot 6H_2O$. The amount of nickel nitrate was calculated to obtain constant nickel surface coverage of 11µmol Ni per m^2 of support, which corresponded to nickel loading of 14, 9.5 and 4 wt.% respectively for alumina, silica and CZ support. Water was removed using rotary-evaporator at 80°C under partial vacuum. Catalyst precursors were subsequently dried overnight at 80°C and calcined in a muffle oven at 450°C for 4h under static air. All catalysts were reduced ex-situ in the stream of H_2 (100cm^3/min STP) at 700°C for 1h in a tubular flow reactor.

2.2. Physico-chemical characterization

Nickel content in prepared materials was determined by ICP analysis.

Structure of prepared materials was analyzed using a PANalytical X'Pert PRO diffractometer equipped with Cu Kα radiation source (λ=0.15418 nm, 40mA, 45kV). The X-Ray diffractograms were registered in 5-90° 2θ range with scan step size 0.017° 2θ and scan step time equal to 35 s. Based on the XRD patterns registered for reduced catalysts the nickel crystallite size was estimated using the Scherrer equation.

Textural parameters (specific surface area, pore volume and mean pore diameter) of prepared catalysts were investigated by low-temperature N_2 sorption experiments with the aid of an ASAP 2020 apparatus from Micromeritics. Samples were outgassed at 250°C overnight prior to analysis. The specific surface area of materials was determined from the Brunauer-Emmet-Teller (BET) equation. The total pore volume was estimated from the N_2 adsorbed volume at p/p_0=0.99.

H_2-TPR profiles were recorded using AutoChem 2920 apparatus from Micromeritics equipped with TC detector. 50 mg of the catalyst sample was heated in a U-tube quartz reactor from room temperature to 1000°C with a heating rate of 10°C/min in a 5% v/v H_2/Ar stream (total flow 40cm^3/min).

The complex permitivity (dielectric constant) of supports and nickel catalysts was measured with the aid of Microwave Dielectric Measurement Kit from ITACA. The prepared materials were pelletized into pellets with 13 or 16mm diameter and minimal height of 5mm. The measurements were performed at room temperature and at a frequency of 2.45 GHz.

2.2.1. In-situ FTIR *adsorption of probe molecules (NO, CO and CO_2)*

In situ FTIR measurements of the different probe molecules i.e. NO, CO and CO_2 on the surface of prepared catalysts were performed with the aid of a NicoletMagna 550 FTIR spectrometer equipped with MCT detector. The FTIR spectra were recorded in the 4000-650cm^{-1} range using 4cm^{-1} optical resolution (32 scans). Catalyst samples were pressed ($1.96 \cdot 10^5$ Pa) into self-supported wafers (2cm^2 ca. 20-30mg). Prior to infrared measurements, the catalyst was activated under secondary vacuum (ca. $6 \cdot 10^{-4}$ Pa) at 350°C for 4h with a heating rate of 3°C/min. The wafers were subsequently cooled down to 150°C (cooling rate 3°C/min) and reduced consecutively two times during 30 min with ca. 130-140 hPa (100 Torr) of H_2. The sample was cooled down to room temperature and the adsorption experiments were performed. Small volume (1.57cm^3) doses (between 0.09-0.9µmol) of probe molecules were sent to the sample until complete surface saturation. CO and NO probe molecules were selected to characterize the nickel metal active phase, while CO_2 was selected to characterize basicity of the supports.

2.3 Plasma-catalytic tests

Prior to each plasma-catalytic or catalytic test, the prepared materials were pelletized and crushed. The fraction characterized by a 1-3mm diameter was selected. Subsequently, materials were reduced ex-situ in the stream of H_2 (100cm^3/min STP) at 700°C for 1h in a tubular flow reactor.

Plasma-catalytic and catalytic tests were performed in a set-up schematically shown in Fig. 1. In a typical test, 3g of catalyst were placed in a Pyrex® glass reactor with 2 cm internal diameter supported on a quartz frit. The catalysts bed was placed between two tungsten electrodes (separated by 13.5 cm) connected to the plasma generator. Gases were supplied through the top of the reactor. The flow of reactant gases was equal to 20cm^3/min (STP) and was controlled by mass flow controllers from BROOKS. The catalyst bed height ranged between 0.5 and 3 cm depending on the bulk densities of prepared materials. The catalysts prior to each test were activated under secondary vacuum at 250°C for 2h. CO_2 methanation was performed using a CO_2/H_2/Ar molar ratio of 2/8/10. The pressure inside the reactor was measured by pressure controllers (Pfeiffer Vacuum) and was within the range 220-270 Pa (1.7-2 Torr). The applied conditions corresponded to GHSV within the range 60,000-360,000h^{-1}.

The catalyst bed was placed between two tungsten electrodes which guaranteed plasma discharge generation through the catalyst bed. Additionally, a heating jacket with cartridge heaters was placed around the glass reactor. The temperature of the catalyst bed was controlled by thermocouple coupled to a PID controller which allowed to perform plasma-catalytic and catalytic tests at elevated temperatures (from room temperature to 300°C).

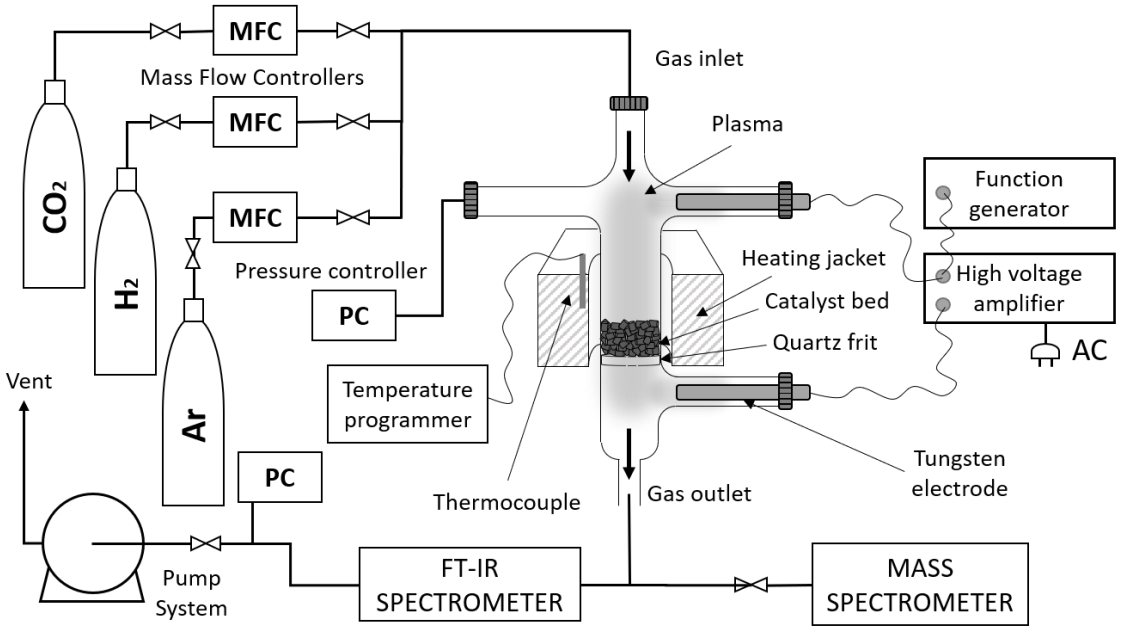

Fig. 1 Scheme of plasma-catalytic set-up used for the evaluation of the performance of prepared materials.

The gases leaving the reactor were analyzed on-line by both infrared spectroscopy (Bruker Vertex 80 v FTIR Spectrometer) and mass spectrometry (Quadrupole Mass Spectrometer, Pfeiffer Omnistar GSD 301). The FTIR spectra were recorded between 4000-1000cm^{-1} with an optical resolution of 0.2cm^{-1}.

Glow discharge plasma was generated with the application of 2 various plasma generators. In the first configuration, the discharge was generated using a plasma function generator (FI5350GA) coupled to a high voltage amplifier (Trek model 20/20C). The function generator generated the pulse signal with the frequency of 66Hz, peak to peak voltage of 3V_{pp} and cycle time of 15 ms with duty of 33% (5ms On and 10 ms OFF). As the generated signal was amplified 2000 times, the final discharge voltage was equal to 6kV with a maximum current of 20 mA. In the second configuration, the plasma discharge was generated by a high voltage AC power supply (Resinblock transformer FART, 50 mA) giving a sinus signal characterized by a 50kHz frequency and 2kV voltage with higher current. The two configurations which differed in the type of generated signal and discharge power will be referred to as Generator 1 and Generator 2 respectively.

The CO_2 conversion, CH_4 and CO yield and carbon balance were calculated from the intensity of the appropriate bands of FT-IR spectra using the following equations:

$$CO_2 \text{ conversion: } X_{CO_2}(\%) = \frac{F_{CO_2,in} - F_{CO_2,out}}{F_{CO_2,in}} \cdot 100\%$$

$$CH_4 \text{ yield: } Y_{CH_4}(\%) = \frac{F_{CH_4,out}}{F_{CO_2,in}} \cdot 100\%$$

CO Yield: $Y_{CO}(\%) = \frac{F_{CO,out}}{F_{CO_2,in}} \cdot 100\%$

Carbon Balance: $CB\ (\%) = \frac{C_{mol,out}}{C_{mol,in}} \cdot 100\% = Y_{CH_4}(\%) + Y_{CO}(\%) + \left(100 - X_{CO_2}(\%)\right)$

3. Results and discussion

3.1. Physico-chemical characterization of the prepared materials

XRD diffractogram acquired for the commercial and prepared supports are presented in Fig. 2 (a). The calcined alumina support was characterized by the crystal structure of γ-Al_2O_3. On the other hand, silica exhibited amorphous structure. The ceria-zirconia support, which was not the commercial material, showed the reflections characteristic for two separate phases of ceria and zirconia. Samples after the introduction of nickel exhibited additional reflections characteristic for cubic nickel oxide phase (Fig. 2 (b) – reflections at 37.2, 43.3, 62.8, 73.4 and 79.4° 2θ), which after reduction in the stream of H_2 transformed into cubic metallic nickel structure (Fig. 2 (c) – reflections at 44.4, 51.7 and 76.1° 2θ).

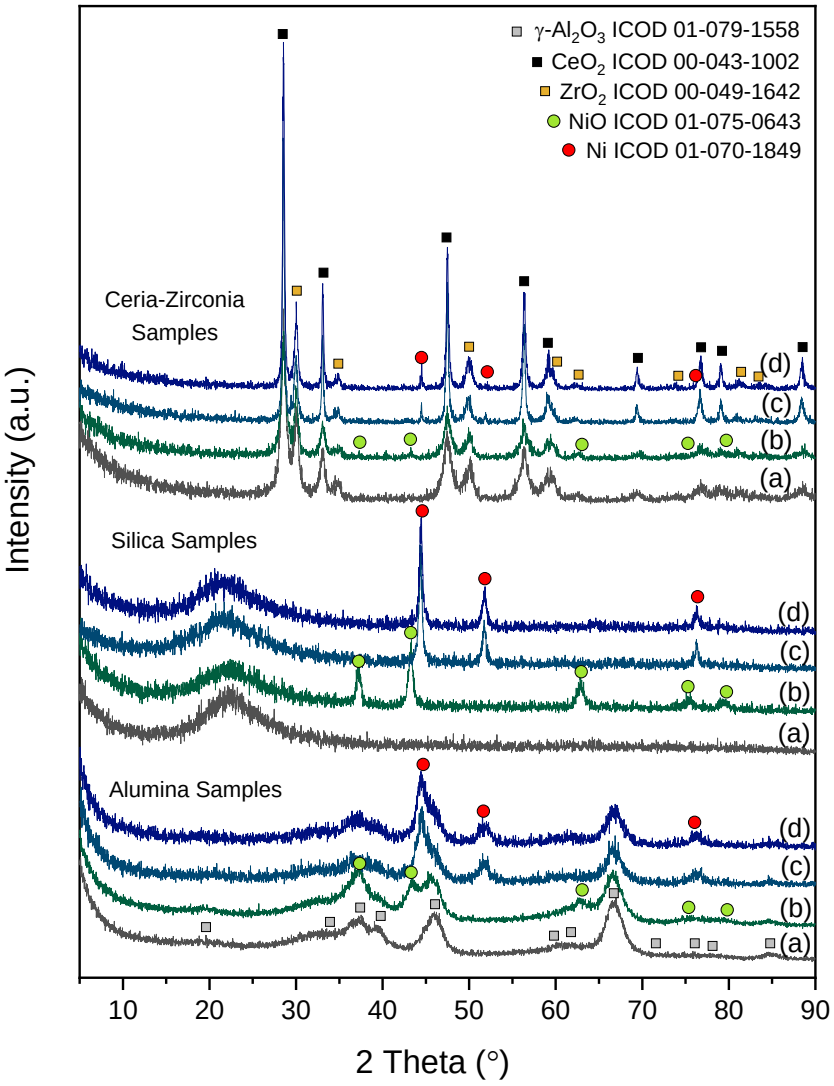

Fig. 2 XRD diffractograms registered for prepared materials: (a) calcined supports, (b) calcined supports with impregnated nickel, (c) reduced materials and (d) catalysts after plasma-catalytic tests

In order to correctly select a reduction temperature of prepared catalysts, H_2-TPR experiments were performed. The registered reduction profiles are presented in Fig. 3 A. The Ni/Al_2O_3 catalyst was characterized by one reduction peak with the maximum at 700°C, suggesting strong nickel-alumina interactions. Nevertheless, the formation of $NiAl_2O_4$ spinel phase was not observed (see Fig. 2(c)). Ni/SiO_2 support showed also one reduction peak with a maximum at 430°C, clearly pointing to much lower interactions of nickel with silica support with respect to Ni/Al_2O_3 sample [43]. This effect is directly reflected in the estimated Ni crystal size obtained from XRD analysis (Table 2). The reduction profile of Ni/CZ sample is more complicated as three reduction regions may be distinguished with maximum temperature at 310, 400 and 870-900°C. Such profile results from overlapping of the reduction of nickel oxide and ceria support. The latter proceeds in three steps: (i) reduction of surface oxygen species (250-300°C) [44], (ii) reduction of surface lattice oxygen (450-600°C) [45] and (iii) total bulk reduction up to 900°C [46]. The Ni/CZ catalyst was loaded with the lowest content of

nickel and its reduction process is partially covered by ceria reduction. Thus it is not so straightforward to conclude about the nickel support interactions. The Scherrer estimation of metallic nickel crystallites suggests weak interactions between Ni species and ceria-zirconia support. This conclusion is supported by the low-temperature N_2 sorption experiments (Table 2) as textural properties of the CZ support were the least developed in comparison to alumina and silica. Based on H_2-TPR profiles the reduction temperature of 700°C was selected, which guaranteed almost complete reduction of nickel species for all catalysts, as confirmed by the calculation (Table 2).

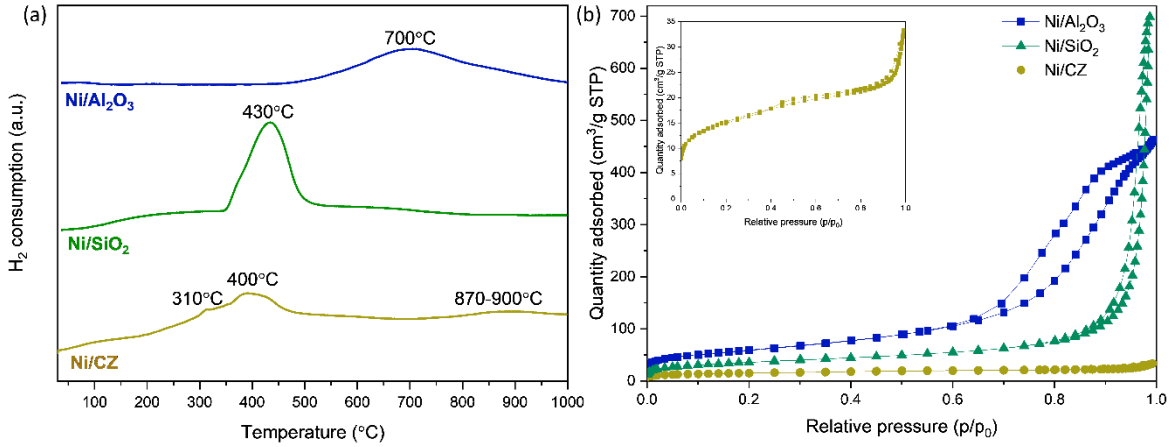

Fig. 3 H_2-TPR profiles (a) and low-temperature N_2 sorption-desorption isotherms (b) registered for the prepared calcined nickel catalysts supported on alumina, silica or ceria-zirconia.

Textural parameters (Table 2) were determined by low-temperature N_2 sorption experiments (Fig. 3(b)). All samples exhibited type IV isotherms characteristic for mesoporous materials. The main difference between samples was in the amount of N_2 adsorbed and type of hysteresis loop, pointing to various pore shape and size distribution [47]. The lowest values of textural parameters were observed for CZ support, which may be explained by the formation of separate ceria and zirconia phases, rather than one ceria-zirconia phase, as confirmed by XRD analysis (Fig. 2). Nevertheless, the obtained values stay in line with the data reported in the literature [48,49]. In the case of all catalysts, values of the specific surface area decreased after nickel species incorporation, pointing to partial blockage of pores. An N_2 uptake increase at high relative pressure may be observed, suggesting the existence of some interparticle mesoporosity. This may explain the increase in total pore volume and mean pore diameter values observed for the Ni/Al_2O_3 sample.

The dielectric constants of the three supports and those of the three nickel doped catalysts are shown in Table 2. For all cases, the dielectric constant of nickel doped catalysts was lower than that of supports (without metal). This fact points out the decrease of the dielectric constant values after the transition metal introduction in agreement with Azzolina-Jury et al. [50]**. Dielectric constants are also highly dependent on the water adsorption capacity of samples. The water**

adsorption capacity trend for the three nickel doped catalysts is: Ni/Al_2O_3 (8.90%wt) > Ni/SiO_2 (8.47%wt) > Ni/CZ (4.27%wt). Ni/Al_2O_3 catalyst presents a higher dielectric constant than Ni/SiO_2 as a consequence of the higher water content during the dielectric constant measurements even if there is 20% more nickel in its structure. However, it was observed that Ni/CZ, with the lowest water adsorption capacity and nickel amount, presented the highest dielectric constant. This fact can be explained through the material density which was 4 times higher than that of the other two catalysts. The Ni/CZ pellet, prepared for dielectric constant measurement, presented a significant lower porosity than that of the other two cases, leading thus to a higher dielectric constant value (with and without metal).

Table 2 Results of physicochemical characterization of prepared catalysts including nickel content, textural and structural parameters, reducibility information and dielectric constant.

Sample	Ni[a] (wt.%)	S_{BET}[b] (m^2/g)	V_{tot}[b] (cm^3/g)	d_r[b] (nm)	Ni crystal size[c] (nm)	T_{max}[d] (°C)	Ni reduced[d] (%)	Dielctric constant[e] ε_r (-)
Ni/Al_2O_3	11.58	214 (248)	0.72 (0.78)	11 (13)	7	700	81	2.58 (3.03)
Ni/SiO_2	9.23	129 (165)	1.08	34	21	430	97	1.79 (2.11)
Ni/CZ	3.45	53 (64)	0.04 (0.04)	5 (4)	>20	310, 400, 870-900	-	5.94 (6.38)

[a] determined by ICP analysis
[b] determined by low-temperature N_2 sorption; in parenthesis are given values registered for the corresponding support
[c] estimated for the reduced samples by the Scherrer equation from the position of Ni(200) reflection
[d] determined by H_2-TPR experiments
[e] measured at 2.45GHz and at ambient temperature; in parenthesis are given values registered for the corresponding support

3.2. Effect of support alone in plasma CO_2 hydrogenation

In the first series of experiments, the effect of the support on the plasma performance was evaluated. The results of the experiments performed with an empty reactor (bars, Fig. 4) and in the presence of 3 studied supports under plasma conditions generated by generator 1 and generator 2 are presented in Fig 4. In the case of all experiments, CO_2 was converted to carbon monoxide. CH_4 production was not observed at all tested temperatures, which points that the presence of nickel metallic phase is necessary to form CH_4. Nevertheless, the presence of various metal oxides in the reactor affects the conversion of CO_2 under plasma conditions. Regardless of the plasma generator applied, the CO_2 conversion followed the sequence: silica > alumina > ceria-zirconia. This stays in line with the values of dielectric constant (see Table 2) and clearly shows that physical properties of supports may greatly influence the performance of the plasma by changing its properties. In the case

of silica and alumina materials, their performance is better when more powerful generator 2 is used. This may be explained by the fact that the more power is supplied to form plasma the more reactive whole system becomes and CO_2 conversion increases. However, this is not the case when ceria-zirconia support is used. Moreover, when a more powerful plasma source is used (generator 2), CO_2 conversion in the presence of ceria-zirconia is even lower than in the case of an empty reactor. The explanation of this phenomenon may be found in the values of the dielectric constant. It is important to underline here that the dielectric constant was measured at the frequency of 2.45 GHz while the experiments were performed using the frequency 66Hz or 50kHz. The CZ support was characterized by 2-3 times higher values of ε_r, which may result in the formation of hot spots in the catalyst bed and thus plasma becomes unstable and the whole system losses activity. The moments in which unstable plasma performance was observed are marked in Fig. 4 in red circles. As it can be seen, the plasma performance becomes unstable when too much energy is supplied into the system, both thermal or electrical.

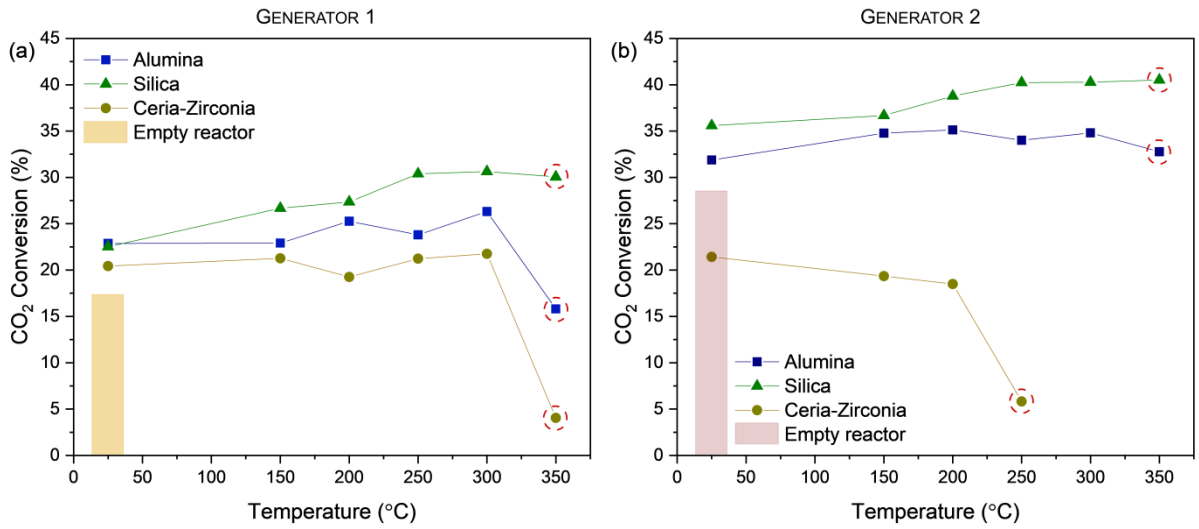

Fig. 4 CO_2 conversion obtained under plasma conditions in the presence of various supports and two different plasma sources: (a) generator 1 and (b) generator 2. (Lines between points are added only to facilitate reading of the graph)

The observed results (Fig. 4) clearly point to the high dependence of plasma performance on the type of material placed inside the reactor. This affects greatly the approach of designing materials for plasma-catalytic processes as the electrical properties of catalyst/supports may affect plasma and thus studies on catalytic processes cannot be directly transferred into the hybrid process. In this case, ceria-zirconia support hindered plasma activity, while in catalytic CO_2 methanation it showed superior performance with respect to alumina and silica. At the same time, it is important to underline that in all cases quartz frit supporting catalyst bed was present inside the reactor (even in case of empty reactor tests) and its electrical properties as well as the irregularity of the materials surface may affect plasma performance as well.

3.3. The catalytic activity of Ni-based catalysts in glow discharge plasma catalytic CO_2 methanation

The CO_2 conversion, CH_4 and CO yield registered for prepared catalysts under glow discharge plasma conditions are presented in Fig. 5, 6 and 7. In case of all samples, CO_2 conversions were following the similar sequence as in the case of the supports, pointing that even in the presence of nickel active phase the support affects CO_2 conversion the most. In terms of CO_2 conversion, the increase in reaction temperature had no beneficial effect, except for Ni/SiO_2 sample (Fig. 6). The most significant differences between catalysts were observed in terms of the products distribution. The Ni/Al_2O_3 catalyst was the most active towards CH_4, followed by the Ni/CZ sample. On the other hand, the Ni/SiO_2 catalyst did not produce methane under plasma. The CH_4 production was affected by the Ni crystal size (Table 2). However, the lack of methane in the products observed over the Ni/SiO_2 catalyst points out that Ni crystal size is not the only factor affecting catalysts activity under plasma-catalytic conditions.

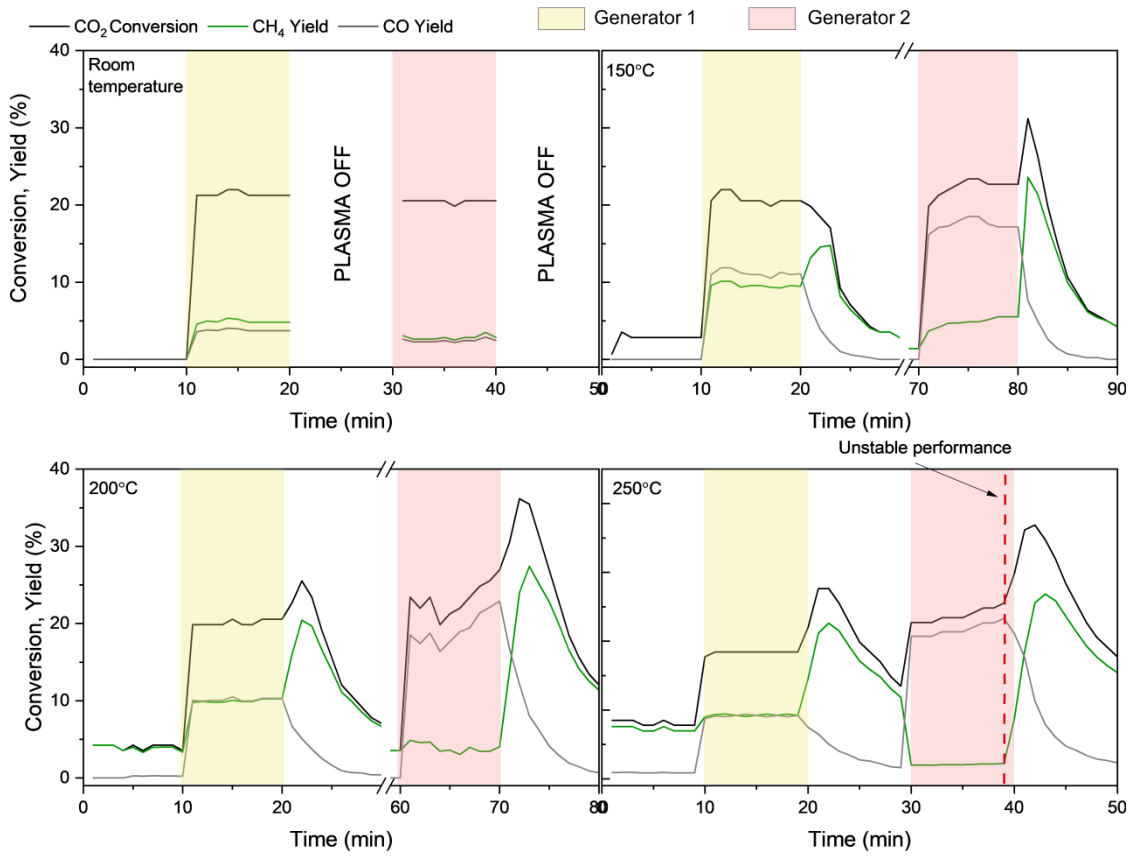

Fig. 5 Results of plasma-catalytic tests performed over the Ni/Al_2O_3 catalyst in the temperature range 25-250°C, low pressure (ca. 2 Torr) and in the presence of 2 plasma generators: Generator 1 (pulse plasma 66Hz, 6kV, 20mA), Generator 2 (sinus plasma 50kHz, 2kV,50mA); $CO_2/H_2/Ar$=2/8/10, total flow 20cm^3/min (STP), m_{cat}=3g;

Methane production depended as well on the plasma power. In general, CH_4 production under plasma conditions was lower when more powerful plasma generator was used, suggesting that

produced CH_4 desorbed from the catalyst surface is subsequently decomposed in plasma. Such effect was already described in the literature. Arita et al. [51] investigated the production of methane in a low-pressure CO_2/H_2 glow discharge with and without a magnetic field. The application of the magnetic field allowed to diffuse electrons to the different reaction region away from neutral radicals. At the same time, the neutral radicals produced in plasma were able to recombine producing CH_4. Such effect reduced CH_4 re-decomposition in plasma and thus increased CH_4 selectivity. Decomposition of produced CH_4 under CO_2 hydrogenation conditions and DBD plasma was as well discussed by de Bie et al. [52].

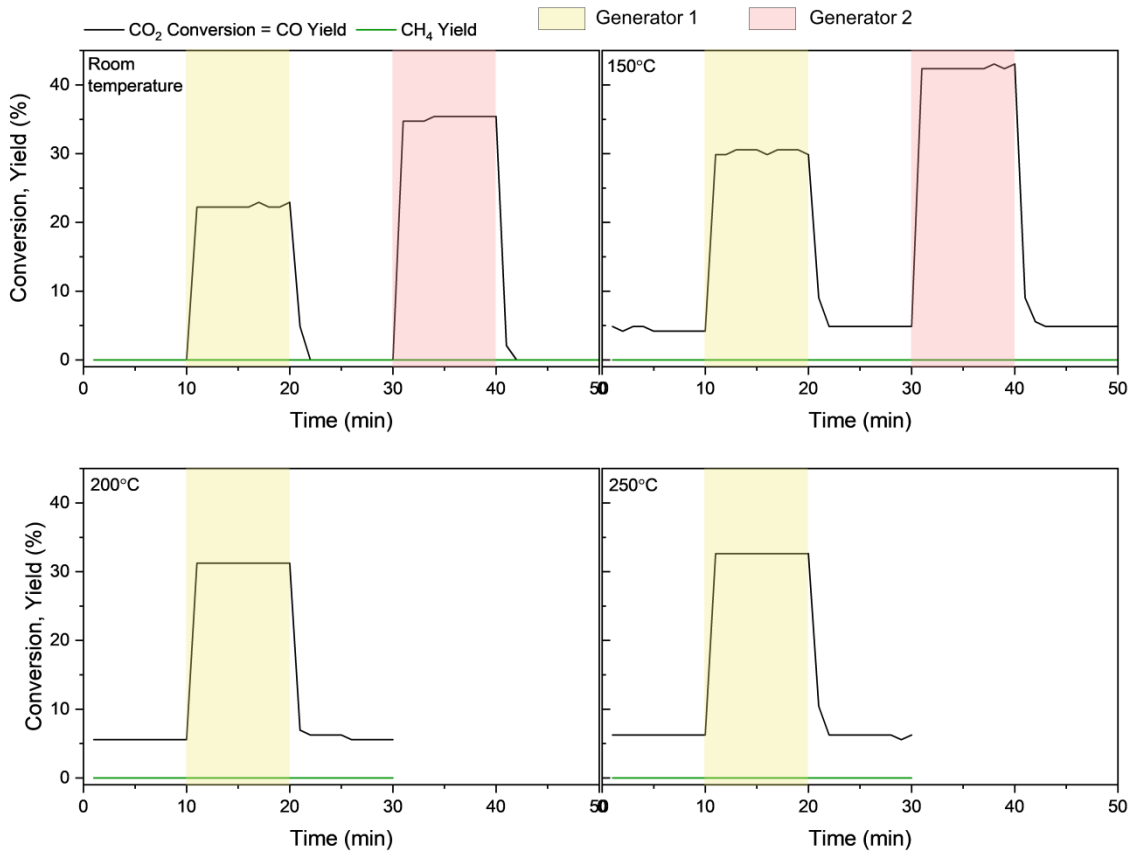

Fig. 6 Results of plasma-catalytic tests performed over the Ni/SiO_2 catalyst in the temperature range 25-250°C, low pressure (ca. 2 Torr) and in the presence of 2 plasma generators: Generator 1 (pulse plasma 66Hz, 6kV, 20mA), Generator 2 (sinus plasma 50kHz, 2kV, 50mA); $CO_2/H_2/Ar$=2/8/10, total flow 20cm^3/min (STP), m_{cat}=3g;

The reaction temperature had a minor effect on catalysts activity towards CO_2 as the registered values of CO_2 conversion were at the same level (Fig. 5-7). However, the reaction temperature as well as the power of the plasma source influenced the stability of the whole system. At high reaction temperatures (above 200°C) and with Generator 2, the formation of hot spots in the catalyst bed was observed, which resulted in a rapid increase of pressure inside the reactor. This may be explained by the sudden and local increase of temperature affecting the steady state of the system.

The plasma was turned off immediately after observation of the hot spot's formation (red dash lines in Fig. 5 and 7).

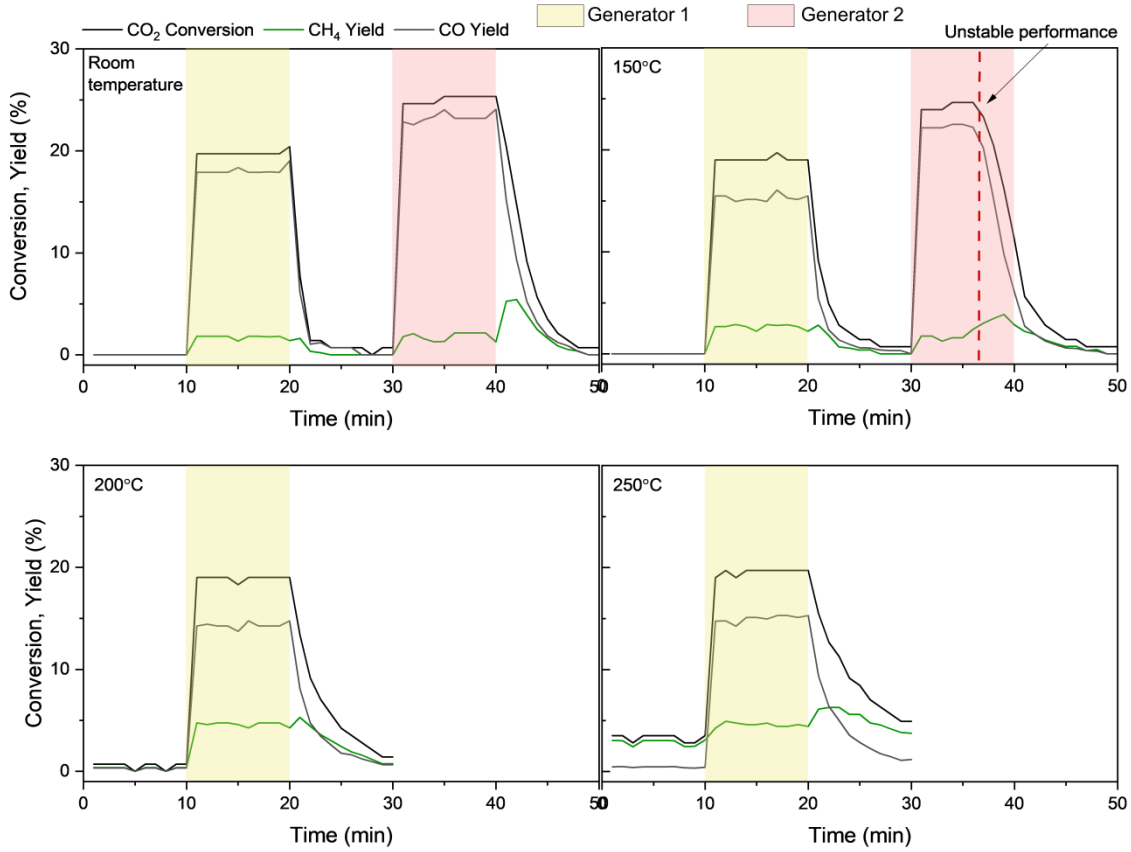

Fig. 7 Results of plasma-catalytic tests performed over the Ni/CZ catalyst in the temperature range 25-250°C, low pressure (ca. 2 Torr) and in the presence of 2 plasma generators: Generator 1 (pulse plasma 66Hz, 6kV, 20mA), Generator 2 (sinus plasma 50kHz, 2kV, 50mA); $CO_2/H_2/Ar=2/8/10$, total flow 20cm^3/min (STP), m_{cat}=3g;

3.3.1. CH_4 production after plasma extinction

The most interesting aspect of the experiments was observed after plasma extinction. In the case of both active catalysts in CH_4 production, i.e. Ni/Al_2O_3 (Fig. 5) and Ni/CZ (Fig. 7), a significant increase after plasma was turned off was observed. This increase of CH_4 production was greater when more energy was put in the system, both in terms of plasma power (Generator 2 > Generator 1) and heat (increase in CH_4 production with the increase in temperature). A similar observation was observed in a previous work by Azzolina-Jury et al. [28] who tested Ni/USY zeolite-based catalysts under low-pressure glow discharge plasma. They explained this effect by the occupation of nickel active sites *via* CO under plasma conditions. After plasma extinction, CO production was stopped, and the coverage of surface nickel species was decreased. This made nickel sites available for H_2 adsorption which resulted in the increased CH_4 production. Moreover, they observed that CH_4 production after plasma extinction was proportional to the nickel reduction degree and nickel content, which is also true for Ni/Al_2O_3 and Ni/CZ catalysts. However, the CO_2 conversion after plasma extinction in the

case of both catalysts does not follow the same trend, suggesting various mechanisms of CH_4 production. Therefore, the increased production of CH_4 might be a result of a combination of various effects, including the one proposed in the work of Azzolina-Jury et al. [28,29]. In the case of Ni/CZ sample, CH_4 production is not accompanied by the increase of CO_2 conversion, as it is in the case of Ni/Al_2O_3 catalyst. At the same time, the carbon balance (results not shown) suggests agglomeration of carbon species under plasma conditions. This carbon agglomeration was proportional to the plasma power applied (Generator 1 or 2). At the same time, an increase in reaction temperature decreased the agglomeration of carbon species during plasma discharge. Most probably, these carbon species are generated through CH_4 decomposition and after plasma extinction they may react with H species producing CH_4. This also stays in line with the results for carbon balance, which confirmed the carbon release after plasma extinction. This suggests that CH_4 production after plasma extinction is a result of the reaction of the species already present on the catalyst surface.

In case Ni/Al_2O_3 CH_4 production after plasma extinction is accompanied by the increasing conversion of CO_2, suggesting that catalyst surface is still active for CO_2 methanation reaction. This effect may be explained by several phenomena. Firstly, under plasma conditions, catalyst surface is bombarded by various species which may modify its surface properties making the surface sites temporary active. The second possibility is the formation of hot spots in the catalyst bed. The temperature around such a hot spot may be high enough to overcome activation energy resulting in CH_4 production. This explanation is additionally supported by the fact that the CH_4 production decreases with time similarly as the hot spot cools down.

3.3.2. Plasma-Catalytic activity vs. electrical properties

Basing on the results presented in section 3.2, it was concluded that CO_2 conversion is dependent on the dielectric constant of material present inside the plasma discharge zone. In order to confirm that statement, the relation between CO_2 conversion obtained using 2 plasma generators in the presence of 3 supports and 3 nickel-based catalysts vs. their dielectric constant were plotted (Fig. 8). This relation is dependent on the plasma power. It seems that for glow discharge plasma produced by generator 1, CO_2 conversion is independent of dielectric properties. However, when more power is supplied to the system (generator 2) then CO_2 conversion shows a negative linear correlation with the increasing dielectric constant. However, this is only true for CO_2 dissociation in plasma and not for CH_4 production. The high correlation (R^2=0.995) was obtained when the points associated with CH_4 production were eliminated (marked in the green circle in Fig. 8) i.e. when part of CO_2 was converted to CH_4. Such situation was observed in the case of Ni/Al_2O_3 and Ni/CZ catalysts.

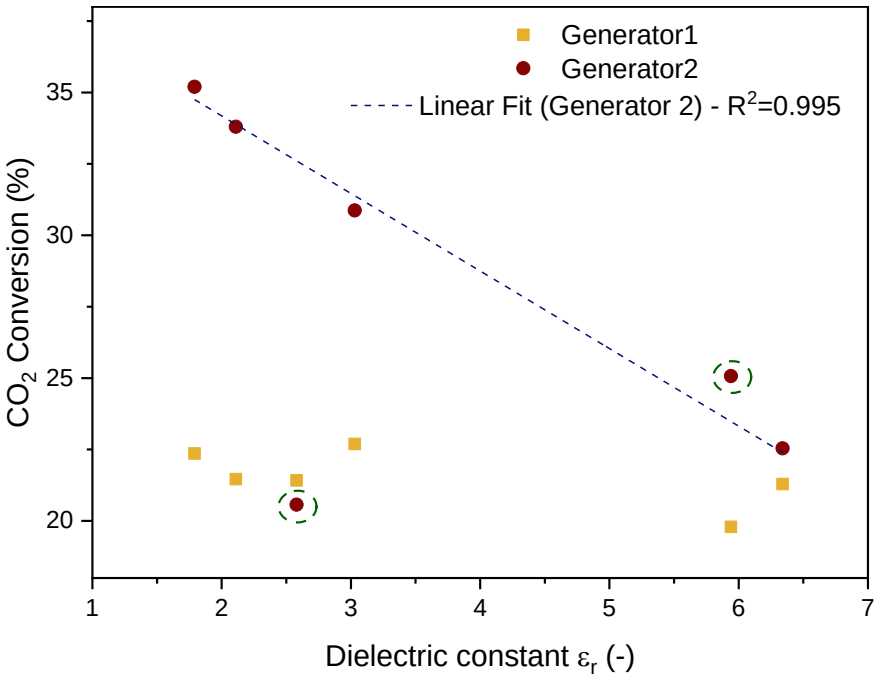

Fig. 8 Relation between CO_2 conversion registered at room temperature and dielectric constant. In green circle were marked points associated with CH_4 production which were not considered for linear fitting of data points.

Interestingly, in literature usually the opposite trend is described. Mora et al. [53] who investigated CO_2/H_2 DBD discharge at atmospheric pressure, showed that better performance in terms of CO_2 conversion was observed when alumina was used as a dielectric when compared to quartz. Bacariza et al. [30] studied various Ni/USY catalysts in DBD atmospheric pressure CO_2 methanation. They observed the better performance of the catalysts characterized by a higher dielectric constant. This was attributed to the enhancement of the electric field caused by the polarization of the catalyst surface and charge accumulation on the dielectric surface, which changes plasma composition. It is important to underline, that these systems were analysed under different conditions with respect to the process presented in this study.

Fig. 8 aims at showing the influence of the dielectric constants of catalysts on the CO_2 conversion via modification of plasma properties such as local electric field intensity changes. However, there are several other parameters affecting the electric field intensity such as the presence of a packed bed within the plasma discharge [54]**. The observed trend on Fig. 8 can be explained *via* the different packed bed void volumes (bed porosity) of the three catalysts. In the case of Ni/CZ the bed porosity is near 4 times lower than in the case of Ni/Al_2O_3 and Ni/SiO_2. Therefore, even if Ni/CZ catalyst presents the higher dielectric constant, the low bed porosity does not allow enhancing the electric field like in the case of the other two catalysts. Moreover, low bed porosity should increase the pressure inside the reactor and affect the plasma properties such as the electron-CO_2 collisions within the gas phase which are responsible for CO_2 dissociation molecules**

by electron impact. This could be a plausible explanation why the catalysts with the highest dielectric constant presented the lowest CO_2 dissociation rate.

3.3.3. Effect of plasma treatment on the thermal catalytic performance

The prepared catalysts were tested as well in the thermal catalytic CO_2 methanation without glow discharge in order to prove the effect of plasma treatment. The results of these tests are presented in Fig. 9 (blank symbols). All samples exhibited better performance in the presence of plasma (Fig, 5-7), both in terms of CO_2 conversion as in the case of CH_4 yield when compared to thermal catalysis (Fig. 9). Under low-pressure conditions and without plasma presence, the catalytic activity in terms of CH_4 production followed the same sequence as under plasma-catalysis i.e. Ni/Al_2O_3 > Ni/CZ >> Ni/SiO_2. The Ni/SiO_2 sample did not produce CH_4 at all, while other 2 catalysts were characterized by methane selectivity over 94% at all tested temperatures. Nevertheless, the obtained CO_2 conversions were lower with respect to the plasma-catalytic tests (Fig. 5 & 7).

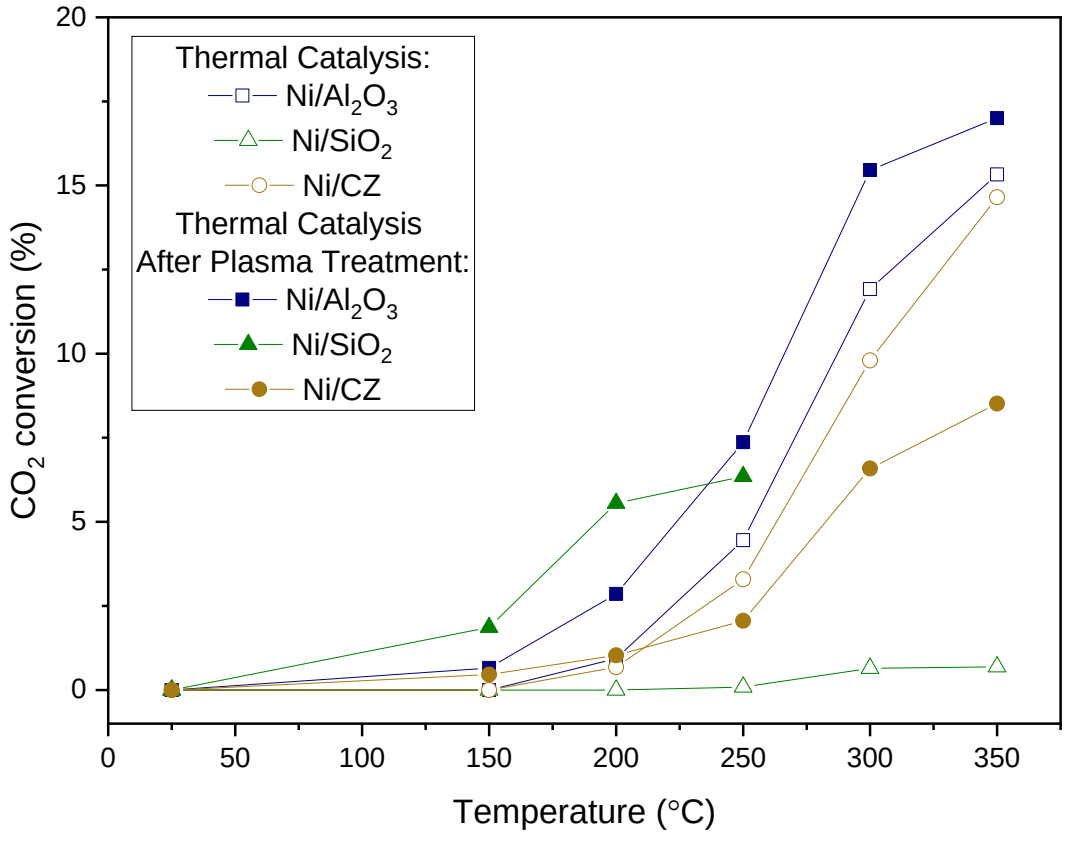

Fig. 9 Results of catalytic CO_2 methanation performed at low pressure for the reduced catalysts (blank symbols) and for the catalysts after plasma treatment (full symbols); $CO_2/H_2/Ar$=2/8/10, total flow 20cm^3/min (STP), m_{cat}=3g; pressure 2 Torr; (Lines between points are added only to facilitate reading of the graph)

In a recent year's catalyst plasma preparation/treatment has gained much attention due to the improvement of catalyst performance [55,56]. For this reason, all prepared catalysts were evaluated in the thermal catalytic CO_2 methanation after plasma-catalytic tests. The results are depicted in

Fig. 9 (full symbols). The comparison of plasma-treated and untreated samples shows that the effect of plasma treatment is dependent on the catalyst properties. For the Ni/Al_2O_3 and Ni/SiO_2 catalysts, a positive effect was observed in terms of CO_2 conversion. The latter sample, however, was still inactive in CO_2 methanation and produced only CO. On the other hand, Ni/CZ catalyst after plasma treatment showed decreased activity.

In literature, the effect of plasma pre-treatment on Ni-based CO_2 methanation catalyst was always positive and was attributed to the increased nickel reducibility and dispersion which also improved H_2 and CO_2 adsorption capacity [39,57–61]. However, in the mentioned reports plasma was used to decompose nickel precursors (usually nickel nitrate) omitting in this way calcination step. In our case, plasma was affecting already reduced nickel catalysts, which resulted in a positive (Ni/Al_2O_3 and Ni/SiO_2) or negative (Ni/CZ) effect of plasma treatment. In order to explain both positive and negative effects of plasma treatment additional characterization experiments were performed (section 3.4).

3.4. FT-IR *in-situ* adsorption of NO, CO and CO_2 – insights into reaction mechanism & effect of plasma promotion

According to the literature [48,62–65], CO_2 methanation may proceed on the catalyst surface *via* 2 proposed paths schematically shown in Fig. 10. The first mechanism involves dissociation of CO_2 to CO which may be further reduced to form surface carbon species. Both adsorbed CO and C may be subsequently hydrogenated to form CH_4. The second proposed mechanism involves direct hydrogenation of adsorbed CO_2 to form formate intermediates which are subsequently transformed to CH_4. In a few publications concerning the mechanism of plasma-catalytic CO_2 methanation, the same reaction mechanisms were proposed [29–31,66]. This proves that the reaction mechanism proceeds *via* the same surface reactions as in case of the thermal catalysts. However, it is important to underline that plasma affects significantly products of the reaction e.g. decomposition of CH_4 as observed in our case (Fig. 5-7). What is more, the plasma may modify catalyst surface, creating new active sites and therefore open a new reaction path.

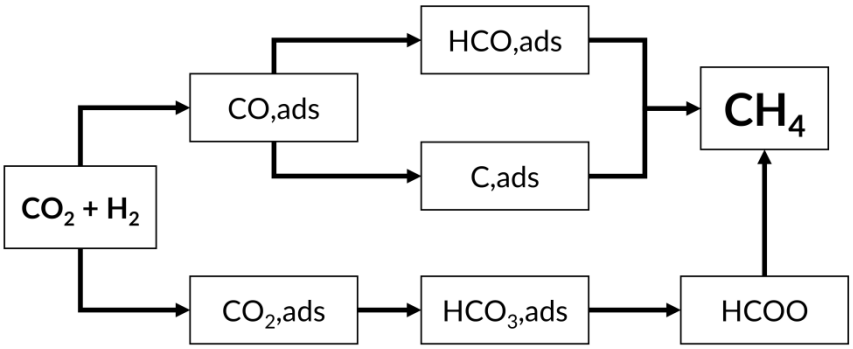

Fig. 10 Scheme of surface reactions involved in CO_2 methanation.

Table 3 Summary of NO, CO and CO_2 adsorption experiments over "freshly" reduced catalysts and samples after plasma-catalytic tests.

Catalyst		**Amount adsorbed (µmol/g)**		
		NO	**CO**	**CO_2**
Ni/Al_2O_3	„fresh"	138	20	51
	Spent	103	25	60
Ni/SiO_2	„fresh"	36	0	12
	Spent	21	0	10
Ni/CZ	„fresh"	8	0	9
	spent	19	11	13

In order to understand the obtained results of plasma-catalytic tests (Fig. 5-7) as well as the effect of plasma treatment in CO_2 methanation (Fig. 9), the reduced catalysts and spent samples after plasma-catalytic tests were characterized by *in-situ* FT-IR adsorption of probe molecules. NO and CO were selected to characterize nickel species, while CO_2 was chosen to evaluate supports basicity. Moreover, CO and CO_2 molecules participate in the reaction, thus they may give insights into the mechanisms of CO_2 methanation. The results of these experiments are summarized in Table 3.

3.4.1. Ni/Al_2O_3

Fig. 11 depicts results of NO, CO and CO_2 FT-IR *in-situ* adsorption experiments performed for reduced and spent Ni/Al_2O_3 catalysts. Samples after adsorption of NO (Fig. 9 a & b) showed 2 absorption bands at 1870 and 1845 cm^{-1} associated with the mono nitrosyl and di nitrosyl species adsorbed on Ni^{2+} sites, respectively [67–69]. The amount of the adsorbed NO species decreased for the spent catalyst (Table 3), indirectly pointing that nickel species were reduced under plasma treatment, which may partially explain the beneficial effect of plasma treatment on Ni/Al_2O_3 sample (Fig. 9).

The CO adsorption revealed the existence of various nickel sites on the catalyst surface. At ca. 2195cm^{-1} absorption band associated with CO adsorbed on Ni^{2+} was observed, confirming the existence of unreduced nickel species. Moreover, the intensity of this band was lower for the spent catalyst, confirming the reduction of Ni^{2+} to Ni^{0} upon plasma treatment Linearly adsorbed carbonyls and subcarbonyl species on metallic nickel sites are identified by bands at 2030-2050 and 2065-2090, respectively. Finally, bridged CO adsorbed species were observed at 1960cm^{-1}. The way of CO adsorption on metallic nickel sites may be associated with the dispersion of nickel. The Ni dispersion is increasing from bridged CO adsorbed on poorly dispersed Ni, through linearly adsorbed CO on moderately dispersed Ni, to finally formation of subcarbonyls on well-dispersed Ni species [70,71]. The performed experiments show that the CO adsorption capacity (Table 3) is at a similar level for reduced and spent catalyst. However, nickel dispersion is changing. The bands associated with well-dispersed nickel species are wider for the spent sample with respect to the reduced catalyst, suggesting an increase of Ni dispersion after the plasma reaction.

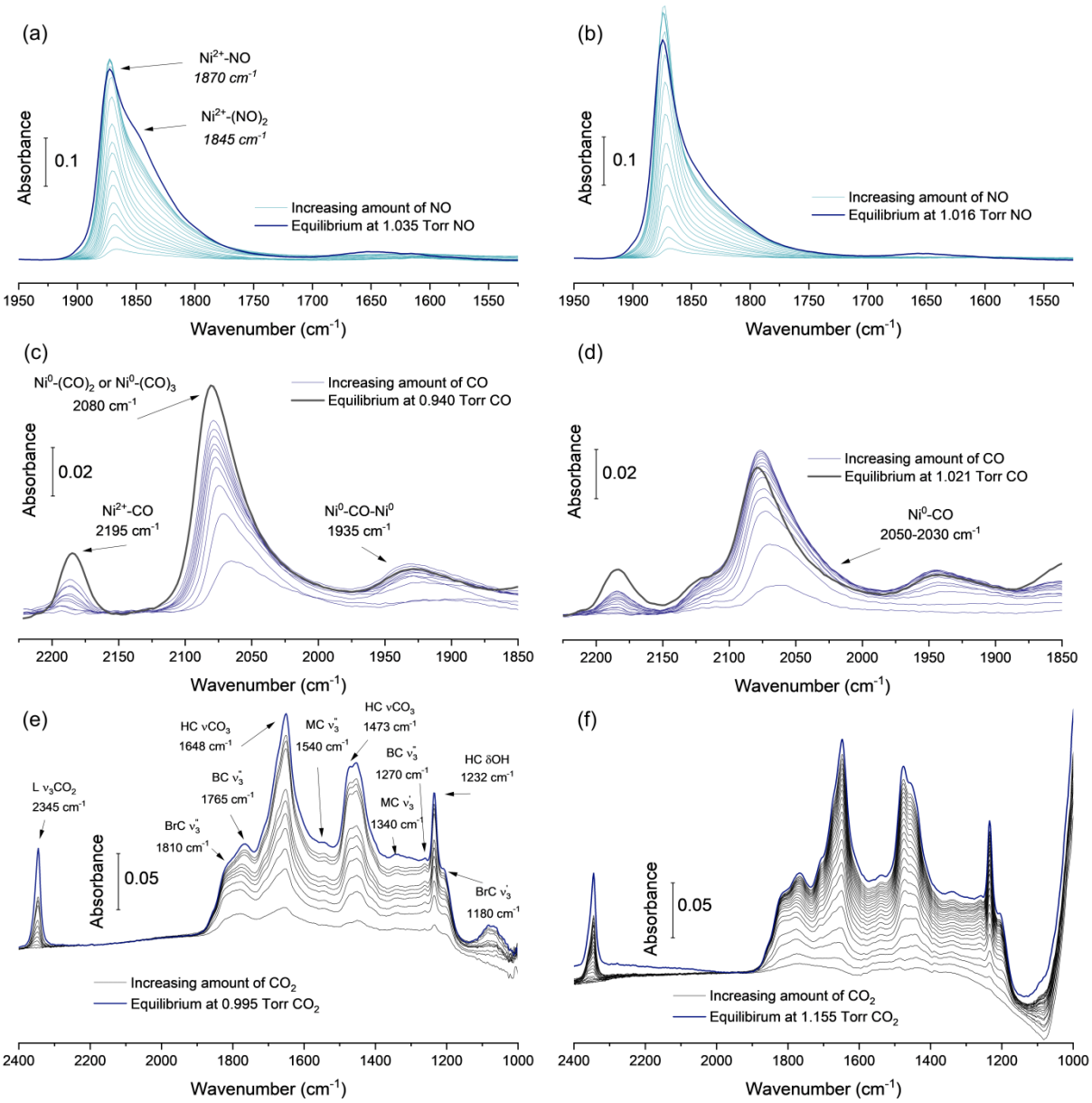

Fig. 11 Adsorption of probe molecules: NO (a & b), CO (c & d) and CO_2 (e & f) on the surface of reduced (a, c & e) Ni/Al_2O_3 and catalyst after plasma-catalytic tests (b, d & f); L – linearly adsorbed CO_2; MC – monodentate carbonate; BC – bidentate carbonate; BrC – Bidentate bridged carbonate; HC -bicarbonate species;

The CO_2 adsorption experiments revealed the existence of various CO_2 adsorbed species on the catalyst surface. The presence of linearly adsorbed CO_2 was confirmed by the band at 2345 cm^{-1}. The asymmetric and symmetric stretching vibrations of bicarbonates were present at 1648 and 1473 cm^{-1}, respectively, while bending vibrations of bicarbonates were observed at 1232 cm^{-1}. The absorption bands of bidentate and monodentate carbonates were observed at 1765, 1270 and 1540, 1340 cm^{-1}, respectively. The presence of bridged carbonate species was confirmed as well (bands at 1810 and 1180cm^{-1}) [72,73].

The CO_2 adsorption capacity was greater for spent catalysts than for fresh one. Similar observations were reported for nickel-based, hydrotalcite-derived catalysts [74], proving that plasma modifies not only the metallic nickel species but also affects support properties. The supports with high CO_2 adsorption capacity are reported to have a beneficial influence on the performance of CO_2 methanation catalyst [2,3]. The support is treated as a pool of CO_2 species available for methanation reaction. This could explain the superior performance of Ni/Al_2IO_3 sample with respect to silica and ceria-zirconia supported materials. However, the mechanistic study of the reaction under DBD plasma conditions with isotopic labelled CO_2 for $Co/CeZrO_4$ catalyst performed by Parastaev et al. [31] showed that the main reaction path involves plasma induced dissociation of CO_2 in the gas phase, followed by the CO adsorption and subsequent surface reactions leading to CH_4. The path in which CO_2 is dissociated on the surface was possible as well, however, its contribution to CH_4 production was lower than in the case of a former one.

The presented results of adsorption experiments give some important information. Firstly, the best performance of Ni/Al_2O_3 catalyst in glow discharge plasma CO_2 methanation may be attributed to the highest adsorption capacities with respect to other catalysts. Secondly, the results of CO and CO_2 adsorption experiments revealed that both reaction paths, involving CO adsorption or CO_2 hydrogenation (Fig. 10), are possible for Ni/Al_2O_3 catalyst. Finally, the glow discharge plasma changed the surface properties of the catalyst. The adsorption capacity of CO_2 was increased, creating more surface sites for the reaction. At the same time, unreduced Ni^{2+} species were reduced under plasma conditions. Ni dispersion was improved as well. All in all, plasma treatment improved catalyst performance in thermal CO_2 methanation.

3.4.2. Ni/SiO_2

The NO adsorption experiments performed for Ni/SiO_2 sample (Fig. 12 a & b) revealed a similar tendency as in the case of Ni/Al_2O_3 catalyst. The NO adsorption on Ni^{2+} sites decreased after plasma treatment, pointing indirectly to the reduction of nickel. However, an additional adsorption band appeared at $1630cm^{-1}$. According to research performed by Mihaylov and Hadjiivanov [68,69], it can be assigned to the nitratospecies.

The most interesting results for Ni/SiO_2 catalyst were obtained when CO was used as a probe molecule (Fig. 12 c & d). The surface of Ni/SiO_2 catalyst did not show any affinity towards carbon monoxide. Considering that the Ni/SiO_2 sample gave 100% selectivity to CO and no CH_4 was produced, the obtained results point that the mechanism of CO_2 methanation must proceed through the hydrogenation of adsorbed CO species. Since there are no sites available for CO adsorption (Fig. 10 c & d) CH_4 is not produced. Therefore, one can assume that the observed CO_2 conversion for

Ni/SiO_2 samples is mainly a result of plasma gas phase CO_2 dissociation to CO. The presence of Ni/SiO_2 affects plasma properties and thus the CO_2 conversion, the contribution of surface reactions may be probably neglected.

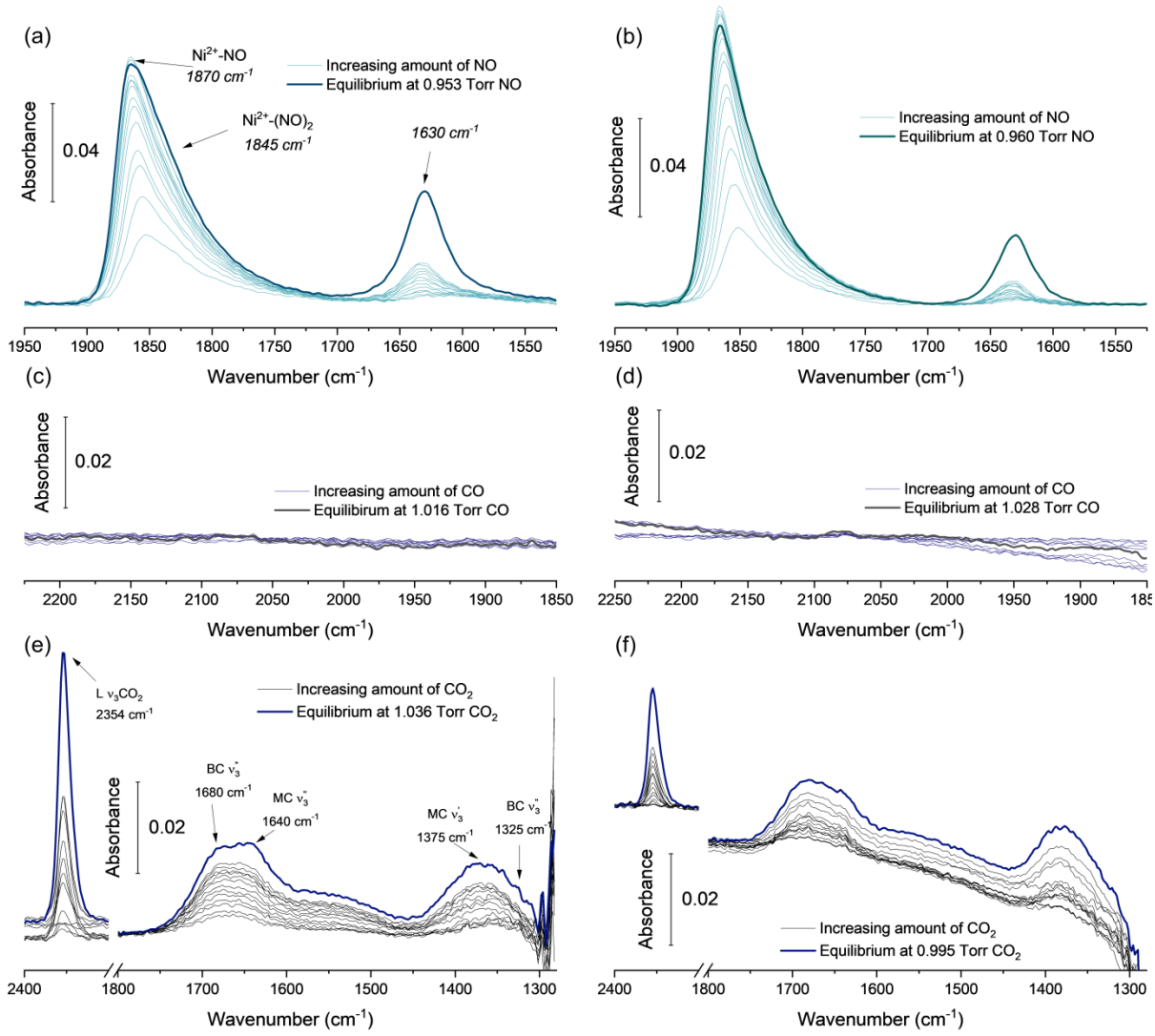

Fig. 12 Adsorption of probe molecules: NO (a & b), CO (c & d) and CO_2 (e & f) on the surface of reduced (a, c & e) Ni/SiO_2 and catalyst after plasma-catalytic tests (b, d & f); L – linearly adsorbed CO_2; MC – monodentate carbonate; BC – bidentate carbonate;

The CO_2 adsorption experiments (Fig. 12 e & f) showed that the CO_2 adsorption capacity is not well developed as well. The CO_2 on the SiO_2 surface was adsorbed mainly in the form of inactive linearly adsorbed species (2354 cm^{-1}). The monodentate (1640 and 1375 cm^{-1}) and bidentate (1680 and 1325 cm^{-1}) species were also observed [75,76]. The CO_2 adsorption capacity after plasma-catalytic tests slightly increased, which may contribute to the positive plasma treatment effect observed for thermal CO_2 methanation (Fig. 7).

3.4.3. Ni/CeO_2-ZrO_2

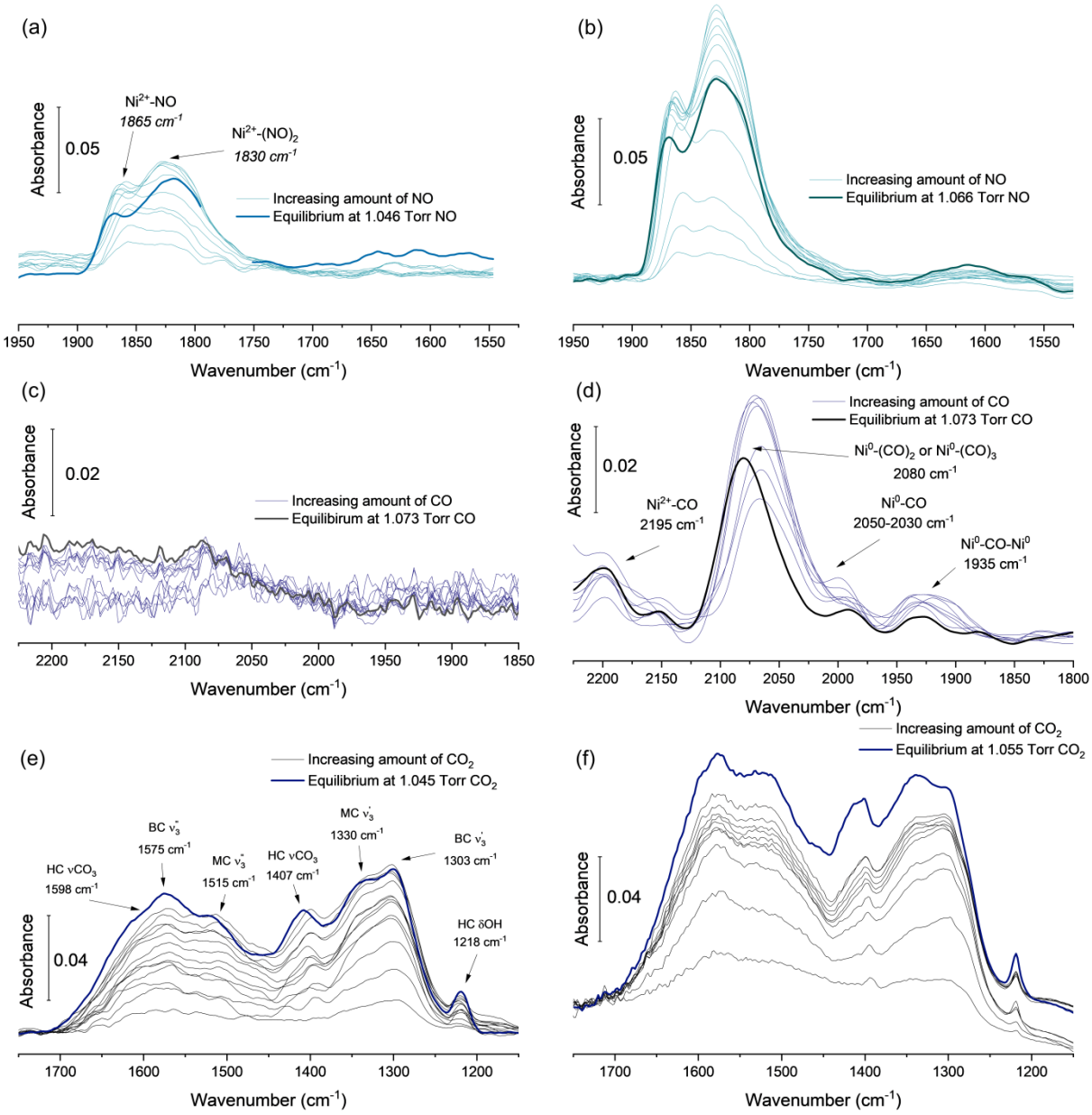

Fig. 13 Adsorption of probe molecules: NO (a & b), CO (c & d) and CO_2 (e & f) on the surface of reduced (a, c & e) Ni/CZ and catalyst after plasma-catalytic tests (b, d & f); MC – monodentate carbonate; BC – bidentate carbonate; HC -bicarbonate species;

Fig. 13 (a & c) shows the results of NO adsorption on Ni/CZ sample, which exhibited 2 absorption bands associated with the NO adsorption on Ni^{2+} sites. In contrast, to Ni/Al_2O_3 and Ni/SiO_2 samples, the intensity of these bands increased for plasma treated sample, suggesting oxidation of Ni^0 species under plasma conditions. Such observation may be explained by the fact that ceria-zirconia is characterized by the existence of mobile oxygen species. Under glow discharge conditions O atoms are formed through CO_2 splitting [77]. They may react with the oxygen vacancies of the CZ support resulting in the support oxidation and subsequent oxidation of nickel species. This explains the

negative effect of plasma treatment on the performance of the Ni/CZ catalyst in the thermal catalysis (Fig. 9).

The reduced Ni/CZ sample did not show any affinity towards CO (Fig. 13 c). The CH_4 production was observed in the case of the thermal catalysis and plasma-catalytic tests for the Ni/CZ sample. This clearly points that CO_2 methanation proceeds through hydrogenation of adsorbed CO_2 (Fig. 10). However, the results of CO adsorption experiments performed for the spent sample (Fig. 13 d) showed the presence of adsorption bands associated with the CO adsorption on both Ni^{2+} and Ni^0. Therefore, plasma treatment activated the sites for CO adsorption. This could open a new reaction path for surface CO_2 methanation via hydrogenation of surface CO species.

The CO_2 adsorption experiments performed for the Ni/CZ samples are presented in Fig. 13 (e & f). For both reduced and spent samples absorption bands associated with the bicarbonates (1598, 1407 and 1218 cm^{-1}), bidentate (1575 and 1303 cm^{-1}) and monodentate (1515 and 1330 cm^{-1}) species were observed [78]. The CO_2 adsorption capacity increased after plasma treatment which could contribute to the improvement of the performance in thermal catalysis. However, as already observed in Section 3.2 the presence of metallic nickel is necessary for CH_4 production. Thus, although CO_2 adsorption was increased, the Ni^0 was oxidized and the overall performance decreased (Fig. 9). The adsorption capacity for plasma treated Ni/CZ sample increased with respect to all examined probe molecules (Table 3). However, this was not transferred for superior performance after plasma treatment.

4. Conclusions

In the presented study the effect of the support on the performance of nickel-based catalysts in a low-pressure glow discharge plasma-catalytic CO_2 methanation was investigated. The nickel loading was normalized to the supports specific surface area to guarantee the same coverage of nickel species on the catalyst surface. The performed experiments revealed that the physicochemical properties of the materials present in the plasma discharge zone influence plasma properties. The correlation between CO_2 conversion and the dielectric constant was found for materials which were not active for CH_4 production, pointing that the presence of catalytically inactive material in the plasma discharge zone affects the reactions in the gas phase.

The catalytic activity in hybrid plasma-catalytic process was greatly dependent on the applied support. It was proven that the support affects plasma properties and thus has an influence on the activation of CO_2. Moreover, it greatly affects the changes of nickel surface species under plasma conditions. Ni/Al_2O_3 catalyst, which exhibited the best performance in terms of CH_4 production, was characterized by the well-developed textural properties (high specific surface area, the high adsorption capacity of both CO_2 and CO) as well as small and well-dispersed nickel crystallites. What is more, these properties were enhanced under plasma conditions, pointing to the beneficial influence of plasma treatment. The Ni/SiO_2 sample turned out to be inactive in glow discharge CO_2 methanation. Its lack of activity was attributed to no adsorption of CO molecules, pointing that the CO_2 methanation over the Ni/SiO_2 catalyst must proceed through the formation of surface carbonyl species. The Ni/CZ catalyst was active in plasma CO_2 methanation. The CO_2 methanation on the Ni/CZ surface may proceed through 2 proposed in literature reaction mechanisms. It was proven that exposure to plasma activates the surface of the Ni/CZ catalyst towards CO adsorption. This, however, was not reflected in the increased CH_4 production, as ceria-zirconia support under plasma conditions oxidizes metallic nickel active sites.

Interestingly, the increased production of CH_4 after plasma extinction was observed for samples active in CO_2 methanation i.e. Ni/Al_2O_3 and Ni/CZ. The obtained results showed that there might be several origins of this CH_4 production. It seems that this effect is as well associated with the properties of the support.

All in all, the presented study showed that the properties of the support greatly influence the performance of catalysts in glow discharge CO_2 methanation.

Acknowledgements

The authors acknowledge the Normandy council for the financial support to RIN CO_2 VIRIDIS project. Authors thank Prof. Sylvain Marinel from CRISMAT laboratory for dielectric constant measurements.

References

[1] V. Masson-Delmotte, P. Zhai, H. O. Pörtner, D. Roberts, J. Skea, P. R. Shukla, A. Pirani, W. Moufouma-Okia, C. Péan, R. Pidcock, S. Connors, J. B. R. Matthews, Y. Chen, X. Zhou, M. I. Gomis,, E. Lonnoy, T. Maycock, M. Tignor, T. Waterfield (eds.), IPCC, Summary for Policymakers, in: Global Warming of 1.5°C. An IPCC Special Report on the Impacts of Global Warming of 1.5°C above Pre-Industrial Levels and Related Global Greenhouse Gas Emission Pathways, in the Context of Strengthening the Global Response to the Threat of Climate Change, Sustainable Development, and Efforts to Eradicate Poverty, World Meteorological Organization, Geneva, Switzerland, 2018.

[2] P. Frontera, A. Macario, M. Ferraro, P. Antonucci, Supported Catalysts for CO2 Methanation: A Review, Catalysts. 7 (2017) 59. doi:10.3390/catal7020059.

[3] K. Ghaib, K. Nitz, F.-Z. Ben-Fares, Chemical Methanation of CO2: A Review, ChemBioEng Reviews. 3 (2016) 266–275. doi:10.1002/cben.201600022.

[4] S. Saeidi, N.A.S. Amin, M.R. Rahimpour, Hydrogenation of CO2 to value-added products—A review and potential future developments, Journal of CO2 Utilization. 5 (2014) 66–81. doi:10.1016/j.jcou.2013.12.005.

[5] I. Kuznecova, J. Gusca, Property based ranking of CO and CO2 methanation catalysts, Energy Procedia. 128 (2017) 255–260. doi:10.1016/j.egypro.2017.09.068.

[6] M. Younas, L. Loong Kong, M.J.K. Bashir, H. Nadeem, A. Shehzad, S. Sethupathi, Recent Advancements, Fundamental Challenges, and Opportunities in Catalytic Methanation of CO2, Energy Fuels. 30 (2016) 8815–8831. doi:10.1021/acs.energyfuels.6b01723.

[7] K. Stangeland, D. Kalai, H. Li, Z. Yu, CO2 Methanation: The Effect of Catalysts and Reaction Conditions, Energy Procedia. 105 (2017) 2022–2027. doi:10.1016/j.egypro.2017.03.577.

[8] B. Eliasson, U. Kogelschatz, B. Xue, L.-M. Zhou, Hydrogenation of Carbon Dioxide to Methanol with a Discharge-Activated Catalyst, Ind. Eng. Chem. Res. 37 (1998) 3350–3357. doi:10.1021/ie9709401.

[9] R. Snoeckx, A. Bogaerts, Plasma technology – a novel solution for CO2 conversion?, Chem. Soc. Rev. 46 (2017) 5805–5863. doi:10.1039/C6CS00066E.

[10] E.C. Neyts, K. (Ken) Ostrikov, M.K. Sunkara, A. Bogaerts, Plasma Catalysis: Synergistic Effects at the Nanoscale, Chem. Rev. 115 (2015) 13408–13446. doi:10.1021/acs.chemrev.5b00362.

[11] E.C. Neyts, A. Bogaerts, Understanding plasma catalysis through modelling and simulation—a review, J. Phys. D: Appl. Phys. 47 (2014) 224010. doi:10.1088/0022-3727/47/22/224010.

[12] J.C. Whitehead, Plasma–catalysis: the known knowns, the known unknowns and the unknown unknowns, J. Phys. D: Appl. Phys. 49 (2016) 243001. doi:10.1088/0022-3727/49/24/243001.

[13] J. Amouroux, S. Cavadias, Electrocatalytic reduction of carbon dioxide under plasma DBD process, J. Phys. D: Appl. Phys. 50 (2017) 465501. doi:10.1088/1361-6463/aa8b56.

[14] A. Bogaerts, T. Kozák, K. van Laer, R. Snoeckx, Plasma-based conversion of CO2: current status and future challenges, Faraday Discuss. 183 (2015) 217–232. doi:10.1039/C5FD00053J.

[15] W.-C. Chung, M.-B. Chang, Review of catalysis and plasma performance on dry reforming of CH4 and possible synergistic effects, Renewable and Sustainable Energy Reviews. 62 (2016) 13–31. doi:10.1016/j.rser.2016.04.007.

[16] W.-C. Chung, I.-Y. Tsao, M.-B. Chang, Novel plasma photocatalysis process for syngas generation via dry reforming of methane, Energy Conversion and Management. 164 (2018) 417–428. doi:10.1016/j.enconman.2018.03.024.
[17] A.H. Khoja, M. Tahir, N.A.S. Amin, Cold plasma dielectric barrier discharge reactor for dry reforming of methane over Ni/ɣ-Al2O3-MgO nanocomposite, Fuel Processing Technology. 178 (2018) 166–179. doi:10.1016/j.fuproc.2018.05.030.
[18] Y. Uytdenhouwen, S. Van Alphen, I. Michielsen, V. Meynen, P. Cool, A. Bogaerts, A packed-bed DBD micro plasma reactor for CO2 dissociation: Does size matter?, Chemical Engineering Journal. 348 (2018) 557–568. doi:10.1016/j.cej.2018.04.210.
[19] G. Chen, V. Georgieva, T. Godfroid, R. Snyders, M.-P. Delplancke-Ogletree, Plasma assisted catalytic decomposition of CO2, Applied Catalysis B: Environmental. 190 (2016) 115–124. doi:10.1016/j.apcatb.2016.03.009.
[20] I. Michielsen, Y. Uytdenhouwen, J. Pype, B. Michielsen, J. Mertens, F. Reniers, V. Meynen, A. Bogaerts, CO2 dissociation in a packed bed DBD reactor: First steps towards a better understanding of plasma catalysis, Chemical Engineering Journal. 326 (2017) 477–488. doi:10.1016/j.cej.2017.05.177.
[21] D. Yap, J.-M. Tatibouët, C. Batiot-Dupeyrat, Carbon dioxide dissociation to carbon monoxide by non-thermal plasma, Journal of CO2 Utilization. 12 (2015) 54–61. doi:10.1016/j.jcou.2015.07.002.
[22] Y. Zeng, X. Tu, Plasma-Catalytic CO2 Hydrogenation at Low Temperatures, IEEE Transactions on Plasma Science. 44 (2016) 405–411. doi:10.1109/TPS.2015.2504549.
[23] Y. Zeng, X. Tu, Plasma-catalytic hydrogenation of CO 2 for the cogeneration of CO and CH 4 in a dielectric barrier discharge reactor: effect of argon addition, J. Phys. D: Appl. Phys. 50 (2017) 184004. doi:10.1088/1361-6463/aa64bb.
[24] M. Nizio, R. Benrabbah, M. Krzak, R. Debek, M. Motak, S. Cavadias, M.E. Gálvez, P. Da Costa, Low temperature hybrid plasma-catalytic methanation over Ni-Ce-Zr hydrotalcite-derived catalysts, Catalysis Communications. 83 (2016) 14–17. doi:10.1016/j.catcom.2016.04.023.
[25] M. Nizio, A. Albarazi, S. Cavadias, J. Amouroux, M.E. Galvez, P. Da Costa, Hybrid plasma-catalytic methanation of CO2 at low temperature over ceria zirconia supported Ni catalysts, International Journal of Hydrogen Energy. 41 (2016) 11584–11592. doi:10.1016/j.ijhydene.2016.02.020.
[26] R. Benrabbah, C. Cavaniol, H. Liu, S. Ognier, S. Cavadias, M.E. Gálvez, P. Da Costa, Plasma DBD activated ceria-zirconia-promoted Ni-catalysts for plasma catalytic CO2 hydrogenation at low temperature, Catalysis Communications. 89 (2017) 73–76. doi:10.1016/j.catcom.2016.10.028.
[27] C.J. Lee, D.H. Lee, T. Kim, Enhancement of methanation of carbon dioxide using dielectric barrier discharge on a ruthenium catalyst at atmospheric conditions, Catalysis Today. 293–294 (2017) 97–104. doi:10.1016/j.cattod.2017.01.022.
[28] F. Azzolina-Jury, D. Bento, C. Henriques, F. Thibault-Starzyk, Chemical engineering aspects of plasma-assisted CO2 hydrogenation over nickel zeolites under partial vacuum, Journal of CO2 Utilization. 22 (2017) 97–109. doi:10.1016/j.jcou.2017.09.017.
[29] F. Azzolina-Jury, F. Thibault-Starzyk, Mechanism of Low Pressure Plasma-Assisted CO<Subscript>2</Subscript> Hydrogenation Over Ni-USY by Microsecond Time-resolved FTIR Spectroscopy, Top Catal. 60 (2017) 1709–1721. doi:10.1007/s11244-017-0849-2.
[30] M.C. Bacariza, M. Biset-Peiró, I. Graça, J. Guilera, J. Morante, J.M. Lopes, T. Andreu, C. Henriques, DBD plasma-assisted CO2 methanation using zeolite-based catalysts: Structure composition-reactivity approach and effect of Ce as promoter, Journal of CO2 Utilization. 26 (2018) 202–211. doi:10.1016/j.jcou.2018.05.013.
[31] A. Parastaev, W.F.L.M. Hoeben, B.E.J.M. van Heesch, N. Kosinov, E.J.M. Hensen, Temperature-programmed plasma surface reaction: An approach to determine plasma-catalytic performance, Applied Catalysis B: Environmental. 239 (2018) 168–177. doi:10.1016/j.apcatb.2018.08.011.

[32] L. Wang, Y. Yi, H. Guo, X. Tu, Atmospheric Pressure and Room Temperature Synthesis of Methanol through Plasma-Catalytic Hydrogenation of CO2, ACS Catal. 8 (2018) 90–100. doi:10.1021/acscatal.7b02733.
[33] S. Tada, T. Shimizu, H. Kameyama, T. Haneda, R. Kikuchi, Ni/CeO2 catalysts with high CO2 methanation activity and high CH4 selectivity at low temperatures, International Journal of Hydrogen Energy. 37 (2012) 5527–5531. doi:10.1016/j.ijhydene.2011.12.122.
[34] Q. Pan, J. Peng, T. Sun, S. Wang, S. Wang, Insight into the reaction route of CO2 methanation: Promotion effect of medium basic sites, Catalysis Communications. 45 (2014) 74–78. doi:10.1016/j.catcom.2013.10.034.
[35] T.A. Le, M.S. Kim, S.H. Lee, T.W. Kim, E.D. Park, CO and CO2 methanation over supported Ni catalysts, Catalysis Today. 293–294 (2017) 89–96. doi:10.1016/j.cattod.2016.12.036.
[36] C. Fukuhara, K. Hayakawa, Y. Suzuki, W. Kawasaki, R. Watanabe, A novel nickel-based structured catalyst for CO2 methanation: A honeycomb-type Ni/CeO2 catalyst to transform greenhouse gas into useful resources, Applied Catalysis A: General. 532 (2017) 12–18. doi:10.1016/j.apcata.2016.11.036.
[37] T.A. Le, M.S. Kim, S.H. Lee, E.D. Park, CO and CO2 Methanation Over Supported Cobalt Catalysts, Top Catal. 60 (2017) 714–720. doi:10.1007/s11244-017-0788-y.
[38] Q. Pan, J. Peng, T. Sun, D. Gao, S. Wang, S. Wang, CO2 methanation on Ni/Ce0.5Zr0.5O2 catalysts for the production of synthetic natural gas, Fuel Processing Technology. 123 (2014) 166–171. doi:10.1016/j.fuproc.2014.01.004.
[39] L. Bian, L. Zhang, Z. Zhu, Z. Li, Methanation of carbon oxides on Ni/Ce/SBA-15 pretreated with dielectric barrier discharge plasma, Molecular Catalysis. 446 (2018) 131–139. doi:10.1016/j.mcat.2017.12.027.
[40] D. Wierzbicki, R. Debek, M. Motak, T. Grzybek, M.E. Gálvez, P. Da Costa, Novel Ni-La-hydrotalcite derived catalysts for CO2 methanation, Catalysis Communications. 83 (2016) 5–8. doi:10.1016/j.catcom.2016.04.021.
[41] D. Wierzbicki, R. Baran, R. Dębek, M. Motak, M.E. Gálvez, T. Grzybek, P. Da Costa, P. Glatzel, Examination of the influence of La promotion on Ni state in hydrotalcite-derived catalysts under CO2 methanation reaction conditions: Operando X-ray absorption and emission spectroscopy investigation, Applied Catalysis B: Environmental. 232 (2018) 409–419. doi:10.1016/j.apcatb.2018.03.089.
[42] S. Rönsch, J. Schneider, S. Matthischke, M. Schlüter, M. Götz, J. Lefebvre, P. Prabhakaran, S. Bajohr, Review on methanation – From fundamentals to current projects, Fuel. 166 (2016) 276–296. doi:10.1016/j.fuel.2015.10.111.
[43] A. Aljishi, G. Veilleux, J.A.H. Lalinde, J. Kopyscinski, The effect of synthesis parameters on ordered mesoporous nickel alumina catalyst for CO2 methanation, Applied Catalysis A: General. 549 (2018) 263–272. doi:10.1016/j.apcata.2017.10.012.
[44] K.Y. Koo, S. Lee, U.H. Jung, H.-S. Roh, W.L. Yoon, Syngas production via combined steam and carbon dioxide reforming of methane over Ni–Ce/MgAl2O4 catalysts with enhanced coke resistance, Fuel Processing Technology. 119 (2014) 151–157. doi:10.1016/j.fuproc.2013.11.005.
[45] C.E. Daza, S. Moreno, R. Molina, Co-precipitated Ni–Mg–Al catalysts containing Ce for CO2 reforming of methane, International Journal of Hydrogen Energy. 36 (2011) 3886–3894. doi:10.1016/j.ijhydene.2010.12.082.
[46] C.E. Daza, J. Gallego, J.A. Moreno, F. Mondragón, S. Moreno, R. Molina, CO2 reforming of methane over Ni/Mg/Al/Ce mixed oxides, Catalysis Today. 133–135 (2008) 357–366. doi:10.1016/j.cattod.2007.12.081.
[47] G. Leofanti, M. Padovan, G. Tozzola, B. Venturelli, Surface area and pore texture of catalysts, Catalysis Today. 41 (1998) 207–219. doi:10.1016/S0920-5861(98)00050-9.
[48] P.A.U. Aldana, F. Ocampo, K. Kobl, B. Louis, F. Thibault-Starzyk, M. Daturi, P. Bazin, S. Thomas, A.C. Roger, Catalytic CO2 valorization into CH4 on Ni-based ceria-zirconia. Reaction mechanism

by operando IR spectroscopy, Catalysis Today. 215 (2013) 201–207. doi:10.1016/j.cattod.2013.02.019.
[49] A. Wolfbeisser, O. Sophiphun, J. Bernardi, J. Wittayakun, K. Föttinger, G. Rupprechter, Methane dry reforming over ceria-zirconia supported Ni catalysts, Catalysis Today. 277 (2016) 234–245. doi:10.1016/j.cattod.2016.04.025.
[50] F. Azzolina Jury, I. Polaert, L. Estel, L.B. Pierella, Synthesis and characterization of MEL and FAU zeolites doped with transition metals for their application to the fine chemistry under microwave irradiation, Applied Catalysis A: General. 453 (2013) 92–101. doi:10.1016/j.apcata.2012.11.046.
[51] K. Arita, S. Iizuka, Production of CH4 in a Low-Pressure CO2/H2 Discharge with Magnetic Field, Journal of Materials Science and Chemical Engineering. 03 (2015) 69. doi:10.4236/msce.2015.312011.
[52] C. De Bie, J. van Dijk, A. Bogaerts, CO2 Hydrogenation in a Dielectric Barrier Discharge Plasma Revealed, J. Phys. Chem. C. 120 (2016) 25210–25224. doi:10.1021/acs.jpcc.6b07639.
[53] E.Y. Mora, A. Sarmiento, E. Vera, Alumina and quartz as dielectrics in a dielectric barrier discharges DBD system for CO 2 hydrogenation, J. Phys.: Conf. Ser. 687 (2016) 012020. doi:10.1088/1742-6596/687/1/012020.
[54] E.C. Neyts, Plasma-Surface Interactions in Plasma Catalysis, Plasma Chem Plasma Process. 36 (2016) 185–212. doi:10.1007/s11090-015-9662-5.
[55] C. Liu, M. Li, J. Wang, X. Zhou, Q. Guo, J. Yan, Y. Li, Plasma methods for preparing green catalysts: Current status and perspective, Chinese Journal of Catalysis. 37 (2016) 340–348. doi:10.1016/S1872-2067(15)61020-8.
[56] C. Liu, G.P. Vissokov, B.W.-L. Jang, Catalyst preparation using plasma technologies, Catalysis Today. 72 (2002) 173–184. doi:10.1016/S0920-5861(01)00491-6.
[57] P. Shi, C.-J. Liu, Characterization of Silica Supported Nickel Catalyst for Methanation with Improved Activity by Room Temperature Plasma Treatment, Catal Lett. 133 (2009) 112. doi:10.1007/s10562-009-0163-0.
[58] X. Zhang, W. Sun, W. Chu, Effect of glow discharge plasma treatment on the performance of Ni/SiO2 catalyst in CO2 methanation, Journal of Fuel Chemistry and Technology. 41 (2013) 96–101. doi:10.1016/S1872-5813(13)60012-2.
[59] L. Bian, L. Zhang, R. Xia, Z. Li, Enhanced low-temperature CO2 methanation activity on plasma-prepared Ni-based catalyst, Journal of Natural Gas Science and Engineering. 27 (2015) 1189–1194. doi:10.1016/j.jngse.2015.09.066.
[60] Z. Fan, K. Sun, N. Rui, B. Zhao, C. Liu, Improved activity of Ni/MgAl2O4 for CO2 methanation by the plasma decomposition, Journal of Energy Chemistry. 24 (2015) 655–659. doi:10.1016/j.jechem.2015.09.004.
[61] R. Zhou, N. Rui, Z. Fan, C. Liu, Effect of the structure of Ni/TiO2 catalyst on CO2 methanation, International Journal of Hydrogen Energy. 41 (2016) 22017–22025. doi:10.1016/j.ijhydene.2016.08.093.
[62] I. Fechete, J.C. Vedrine, Nanoporous materials as new engineered catalysts for the synthesis of green fuels, Molecules. 20 (2015) 5638–5666. doi:10.3390/molecules20045638.
[63] A. Karelovic, P. Ruiz, Mechanistic study of low temperature CO2 methanation over Rh/TiO2 catalysts, Journal of Catalysis. 301 (2013) 141–153. doi:10.1016/j.jcat.2013.02.009.
[64] W. Wei, G. Jinlong, Methanation of carbon dioxide: an overview, Front. Chem. Sci. Eng. 5 (2011) 2–10. doi:10.1007/s11705-010-0528-3.
[65] E. Baraj, S. Vagaský, T. Hlinčík, K. Ciahotný, V. Tekáč, Reaction mechanisms of carbon dioxide methanation, Chem. Pap. 70 (2016) 395–403. doi:10.1515/chempap-2015-0216.
[66] F. Azzolina-Jury, Novel boehmite transformation into γ-alumina and preparation of efficient nickel base alumina porous extrudates for plasma-assisted CO2 methanation, Journal of Industrial and Engineering Chemistry. (2018). doi:10.1016/j.jiec.2018.11.053.

[67] C. Drouet, P. Alphonse, A. Rousset, IR spectroscopic study of NO and CO adsorptions on nonstoichiometric nickel–copper manganites, Phys. Chem. Chem. Phys. 3 (2001) 3826–3830. doi:10.1039/B101523K.
[68] K.I. HADJIIVANOV, Identification of Neutral and Charged N x O y Surface Species by IR Spectroscopy, Catalysis Reviews. 42 (2000) 71–144. doi:10.1081/CR-100100260.
[69] M. Mihaylov, K. Hadjiivanov, FTIR Study of CO and NO Adsorption and Coadsorption on Ni-ZSM-5 and Ni/SiO2, Langmuir. 18 (2002) 4376–4383. doi:10.1021/la015739g.
[70] C.H. Bartholomew, R.B. Pannell, The stoichiometry of hydrogen and carbon monoxide chemisorption on alumina- and silica-supported nickel, Journal of Catalysis. 65 (1980) 390–401. doi:10.1016/0021-9517(80)90316-4.
[71] K.I. Hadjiivanov, G.N. Vayssilov, Characterization of oxide surfaces and zeolites by carbon monoxide as an IR probe molecule, in: Advances in Catalysis, Academic Press, 2002: pp. 307–511. doi:10.1016/S0360-0564(02)47008-3.
[72] K. Coenen, F. Gallucci, B. Mezari, E. Hensen, M. van Sint Annaland, An in-situ IR study on the adsorption of CO2 and H2O on hydrotalcites, Journal of CO2 Utilization. 24 (2018) 228–239. doi:10.1016/j.jcou.2018.01.008.
[73] G. Ramis, G. Busca, V. Lorenzelli, Low-temperature CO2 adsorption on metal oxides: spectroscopic characterization of some weakly adsorbed species, Materials Chemistry and Physics. 29 (1991) 425–435. doi:10.1016/0254-0584(91)90037-U.
[74] R. Debek, D. Wierzbicki, M. Motak, M.E. Galvez, P.D. Costa, F.A. JURY, Operando FT-IR study on basicity improvement of Ni(Mg,Al)O hydrotalcite-derived catalysts promoted by glow plasma discharge, Plasma Sci. Tech. (2018). doi:10.1088/2058-6272/aaf759.
[75] R. Bal, B.B. Tope, T.K. Das, S.G. Hegde, S. Sivasanker, Alkali-Loaded Silica, a Solid Base: Investigation by FTIR Spectroscopy of Adsorbed CO2 and Its Catalytic Activity, Journal of Catalysis. 204 (2001) 358–363. doi:10.1006/jcat.2001.3402.
[76] F. Solymosi, H. Knozinger, Infrared spectroscopic study of the adsorption and reactions of CO2 on K-modified Rh/SiO2, Journal of Catalysis. 122 (1990) 166–177. doi:10.1016/0021-9517(90)90268-O.
[77] J.-Y. Wang, G.-G. Xia, A. Huang, S.L. Suib, Y. Hayashi, H. Matsumoto, CO2 Decomposition Using Glow Discharge Plasmas, Journal of Catalysis. 185 (1999) 152–159. doi:10.1006/jcat.1999.2499.
[78] G. Jacobs, R.A. Keogh, B.H. Davis, Steam reforming of ethanol over Pt/ceria with co-fed hydrogen, Journal of Catalysis. 245 (2007) 326–337. doi:10.1016/j.jcat.2006.10.018.